or more of ganglioside complexes as shown in the Table: GD1a/GM1, GD1b/GT1b, and GM1/GT1b. We plan to investigate intensively the presence of antibodies to the various ganglioside complexes using sera from a larger group of GBS patients.

In view of characteristics of glycosphingolipids forming clusters extensively in the plasma membrane,[7] it is no wonder that clustered glycoepitopes of ganglioside complexes in the membrane are targeted by serum antibodies in GBS patients. No studies, however, have ever found antibodies to the ganglioside complex in sera from patients with GBS and related disorders. OD values of the anti–GD1a/GD1b antibodies were much higher than those of the anti–GD1a or anti–GD1b antibodies, and anti–GD1a/GD1b antibody–positive sera often showed little or no reactivity to GD1a or GD1b in the ELISAs (see Table), indicative that mixing GD1a with GD1b produced a ganglioside complex and new glycoepitopes that differ from those of GD1a or GD1b alone. What the structure of these glycoepitopes formed in the GD1a and GD1b mixture has yet to be determined.

Glycosphingolipids penetrate the outer leaflet of the plasma membrane via ceramide and are preferentially packaged with cholesterol, forming lipid rafts. These lipid rafts, protein-linked microdomains in the plasma membrane, are called detergent-insoluble glycolipid-enriched complexes or glycosphingolipid-enriched membranes. Within the plasma membrane microdomains, glycosphingolipids, particularly gangliosides, are believed to interact with important transmembrane receptors or signal transducers involved in cell adhesion and signaling.[7,8] Because proteins in the microdomains are not free to spread over the plasma membrane, specific ones tend to be concentrated within microdomains that often are essential for protein function. Antibodies to a ganglioside complex therefore may alter the function of the axon or Schwann cell through their binding to clustered epitopes of glycosphingolipids in the plasma membrane microdomains. Consequently, they may directly induce nerve conduction failure and severe disability in patients with GBS.

Some antiganglioside antibodies are correlated with the clinical phenotypes of GBS[2]; an anti–GQ1b antibody is associated with Miller Fisher syndrome[9] and the anti–GM1, GD1a, and GalNAc-GD1a antibodies with pure motor type of GBS.[6,10–13] Anti–GD1a/GD1b antibody also may be correlated with a GBS phenotype. Anti–GD1a/GD1b antibody–positive patients with GBS tend to have severe disabilities and cranial nerve deficits. Clinical studies of larger numbers of patients with GBS are needed to clarify the clinical importance of anti–GD1a/GD1b antibody.

This work was supported by the Ministry of Education, Culture, Sports, Science and Technology of Japan (Grants-in-Aid for Scientific Research, 14570581, 16590854, S.K.), Research Grant for Neuroimmunological Diseases (S.K.), and the Ministry of Health, Labour, and Welfare of Japan (Health Sciences Research Grant on Psychiatric and Neurological Diseases and Mental Health, H15-015, S.K.)

References

1. Kusunoki S, Iwamori M, Chiba A, et al. GM1b is a new member of antigen for serum antibody in Guillain-Barré syndrome. Neurology 1996;47:237–242.
2. Willison HJ, Yuki N. Peripheral neuropathies and anti-glycolipid antibodies. Brain 2002;125:2591–2625.
3. Kaida K, Kusunoki S, Kamakura K, et al. GalNAc-GD1a in human peripheral nerve. Target sites of anti-ganglioside antibody. Neurology 2003;61:465–470.
4. Asbury AK, Cornblath DR. Assessment of current diagnostic criteria for Guillain-Barré syndrome. Ann Neurol 1990;27(suppl): S21–S24.
5. Kusunoki S, Chiba A, Kon K, et al. N-acetylgalactosaminyl GD1a is a target molecule for serum antibody in Guillain-Barré syndrome. Ann Neurol 1994;35:570–576.
6. Kaida K, Kusunoki S, Kamakura K, et al. Guillain-Barré syndrome with antibody to a ganglioside, N-acetylgalactosaminyl GD1a. Brain 2000;123:116–124.
7. Hakomori S. The glycosynapse. Proc Natl Acad Sci USA 2002; 99:225–232.
8. Simons K, Ikonen E. Functional rafts in cell membranes. Nature 1997;387:569–572.
9. Chiba A, Kusunoki S, Shimizu T, Kanazawa I. Serum IgG antibody to ganglioside GQ1b is a possible marker of Miller Fisher syndrome. Ann Neurol 1992;31:677–679.
10. Hadden RDM, Cornblath DR, Hughes RAC, et al. Electrophysiological classification of Guillain-Barré syndrome: clinical associations and outcome. Ann Neurol 1998;44:780–788.
11. Ho TW, Willison HJ, Nachamkin I, et al. Anti-GD1a antibody is associated with axonal but not demyelinating forms of Guillain-Barré syndrome. Ann Neurol 1999;45:168–173.
12. Hao Q, Saida T, Yoshino H, et al. Anti-GalNAc-GD1a antibody-associated Guillain-Barré syndrome with a predominantly distal weakness without cranial nerve impairment and sensory disturbance. Ann Neurol 1999;45:758–768.
13. Ang CW, Yuki N, Jacobs BC, et al. Rapidly progressive, predominantly motor Guillain-Barré syndrome with anti-GalNAc-GD1a antibodies. Neurology 1999;53:2122–2127.
14. Hughes R, Newsom-Davis J, Perkin G, Pierce J. Controlled trial of prednisolone in acute polyneuropathy. Lancet 1978;2: 750–775.

Anti-GQ1b antibody as a factor predictive of mechanical ventilation in Guillain–Barré syndrome

K. Kaida, MD, PhD; S. Kusunoki, MD, PhD; M. Kanzaki, MD; K. Kamakura, MD, PhD; K. Motoyoshi, MD, PhD; and I. Kanazawa, MD, PhD

Abstract—Compared with 87 unventilated patients with Guillain–Barré syndrome (GBS), 44 ventilated patients with GBS more frequently had multiple cranial nerve involvement (91 vs 50%; $p < 0.001$) and IgG anti-GQ1b antibody (27 vs 8%; $p = 0.006$). In GBS patients without ophthalmoparesis, the presence of IgG anti-GQ1b antibody was associated with respiratory failure (12 [3/25] vs 0% [0/67]; $p = 0.04$). The presence of the antibody may be a factor predictive of respiratory failure in GBS.

NEUROLOGY 2004;62:821–824

Poor prognosis for disabilities and prolonged recovery are common for ventilated patients with Guillain–Barré syndrome (GBS).[1,2] Comparison of clinical features between ventilated and unventilated patients with GBS has identified factors predictive of progression to mechanical ventilation,[1,2] leading to an appropriate choice of therapy and improvement of prognoses in patients with severe GBS. Antiganglioside antibodies, which are frequently present in the acute-phase GBS sera, may be immunologic markers associated with certain neurologic features.[3] We investigated the clinical features of and antiganglioside antibodies in ventilated and unventilated patients with GBS to determine factors predictive of progression to artificial ventilation.

Methods. *Study population.* Between January 1998 and September 2000, acute-phase GBS sera, collected from 329 patients with GBS at various general and teaching hospitals throughout Japan, were sent to us. Those sera were obtained on admission and before treatment. Patients' clinical data, also sent to us at that time, were examined by neurologists. The GBS diagnosis was defined clinically by the criteria of Asbury and Cornblath.[4] Those with clinically defined GBS were divided into two groups: ventilated (GBS-AV[+] group) and unventilated patients. Control patients (GBS-AV[−] group) were selected systematically (one in every three consecutive cases in our files) from unventilated patients with GBS to reduce the effects of selection bias. Clinical and electrophysiologic features of the GBS-AV(+) and GBS-AV(−) patients were analyzed.

Analyses of clinical and electrophysiologic features. Patient disabilities were graded on the Hughes Functional Grading Scale.[5] Neurologic symptoms were analyzed during the course of the disease. Electrophysiologic data were evaluated as described previously[6] and categorized as "primary demyelinating," "primary axonal," "inexcitable," "equivocal," or "normal."

Analyses on antiganglioside antibodies. Serum antibodies to nine ganglioside antigens (GalNAc-GD1a, GM1, GM2, GM3, GD1a, GD1b, GD3, GT1b, and GQ1b) were investigated by ELISA, as described elsewhere.[6] IgG anti-GT1a antibody was also investigated in some patients' sera. GalNAc-GD1a was prepared in our laboratory from bovine brain.[6] The other gangliosides were purchased from Sigma (St. Louis, MO).

Statistical analysis. Differences in proportions were tested by Fisher exact probability test or the χ^2 test. The Student t-test was used to compare ages and the Mann–Whitney test to compare onset with nadir (days) of the GBS-AV(+) and GBS-AV(−) groups. The time of nadir, when a patient was most severely affected, was determined by each attending physician. Frequency of antiganglioside antibody was analyzed with a multiple logistic regression model. The dependent variable was artificial ventilation, and the independent variables were IgG anti-ganglioside antibodies that were positive in the sera of >3 patients in 131 total subjects. Two-tailed p values of <0.05 were considered significant. These analyses were performed with StatView (SAS, Cary, NC) and Statistica (3.0; Statsoft, OK) software.

Results. *Study population.* Of 329 patients with clinically defined GBS, 44 (13%) required artificial ventilation (GBS-AV[+] group). Of the 285 unventilated GBS patients, 94 were selected systematically as described in Methods, 7 of whom were excluded because of incomplete clinical data. The GBS-AV(−) group therefore consisted of 57 unventilated male and 30 unventilated female patients with GBS. No significant differences were found between the two groups as to gender and age.

Clinical and electrophysiologic features. Clinical features of the patients in the two groups are given in table 1. Most of the GBS-AV(+) patients had cranial nerve deficits, in particular facial and bulbar palsies (see table 1). Thirty-one GBS-AV(+) patients had more than two of the extraocular, facial, and bulbar palsies. There was no difference between the two groups in the distribution of limb weak-

From the Third Department of Internal Medicine (Drs. Kaida, Kanzaki, Kamakura, and Motoyoshi), National Defense Medical College, Saitama-ken, Department of Neurology (Dr. Kusunoki), Kinki University School of Medicine, Osaka, and Department of Neurology (Dr. Kanazawa), School of Medicine, University of Tokyo, Japan.

Supported in part by a grant-in-aid for scientific research (14570581) from the Ministry of Education, Culture, Sports, Science, and Technology of Japan and a research grant for neuroimmunological diseases and a health sciences research grant (Research on Psychiatric and Neurologic Diseases and Mental Health) from the Ministry of Health, Labor, and Welfare of Japan.

Received January 23, 2003. Accepted in final form October 23, 2003.

Address correspondence and reprint requests to Dr. S. Kusunoki, Department of Neurology, Kinki University School of Medicine, 377-2 Ohno-Higashi, Osaka-Sayama, 589-8511 Japan; e-mail: kusunoki-tky@umin.ac.jp

Table 1 Clinical features of and electrophysiological findings for GBS patients with and without artificial ventilation

Clinical features	GBS-AV(+), n = 44	GBS-AV(−), n = 87	*p* Value*	Odds ratio
Age, y; mean (95% CI)	42 (36–48)	41 (38–45)†	0.8‡	
Male, no. (%)	27 (61)	57 (66)	>0.9	
Antecedent infections, no. (%)	§	‖		
RT	26 (60)	45 (56)	0.54	
GI	7 (16)	24 (30)	0.2	
Onset to nadir, d	¶	**		
Mean (95% CI)	5.9 (5.0–6.8)	6.8 (5.8–7.9)	0.74††	
Cranial nerve deficits, no. (%)	§	‡‡		
Positive	39 (91)	41 (50)	<0.0001	9.8
III, IV, VI	19 (44)	15 (18)	0.004	3.5
VII	33 (77)	25 (30)	<0.0001	7.5
IX, X	28 (65)	28 (34)	0.002	3.6
XI	6 (14)	1 (1)	0.01	13
XII	8 (19)	4 (5)	0.04	4.5
Sensory disturbances, no. (%)	§§	‖‖		
No	11 (28)	20 (25)	0.87	
Sensory loss	13 (33)	31 (39)	0.71	
Electrophysiology, no. (%)	‖‖	¶¶		
Primary demyelinating	16 (52)	22 (58)	>0.9	
Primary axonal	2 (7)	3 (8)	>0.9	
Inexcitable	3 (10)	0 (0)	0.17	
Normal	0 (0)	2 (5)	0.6	
Equivocal	10 (32)	11 (29)	>0.9	

* Two-tailed *p* value; † n = 85; ‡ Student *t*-test; § n = 43; ‖ n = 80; ¶ n = 36; ** n = 73; †† Mann–Whitney *U* test; ‡‡ n = 82; §§ n = 39; ‖‖ n = 31; ¶¶ n = 38.

GBS = Guillain–Barré syndrome; AV = artificial ventilation; RT = respiratory tract infection; GI = gastrointestinal tract infection.

ness and sensory disturbance. Detailed information on autonomic dysfunction was not obtained. Electrophysiologic findings were "primary demyelinating" type dominant in both groups (see table 1).

Treatment and prognosis. Treatment and prognosis in GBS-AV(+) and GBS-AV(−) groups are summarized in table 2. GBS-AV(+) group patients tended to be treated more extensively than GBS-AV(−) group patients. Because the long-term follow-up data often were incomplete, short-term prognoses were evaluated (see table 2).

Frequencies of antiganglioside antibodies. Antiganglioside antibody frequencies in the GBS-AV(+) and GBS-AV(−) groups are shown in table 3. IgG anti-GQ1b and anti-GT1a antibodies occurred significantly more often in the GBS-AV(+) group. The frequency of anti-GQ1b antibodies in GBS-AV(+) patients with ophthalmoparesis (9/19 = 47.4%) equaled that in GBS-AV(−) patients with ophthalmoparesis (7/15 = 46.7%), with no significance ($p > 0.9$, χ^2 test). The frequency of anti-GQ1b antibodies in GBS-AV(+) patients without ophthalmoparesis (3/25 = 12%) was higher than that in GBS-AV(−) patients without ophthalmoparesis (0/67 = 0%; $p = 0.04$, Fisher exact probability). As for the frequency of IgG anti-GT1a antibody, however, there were no such significant differences: GBS-AV(+) with ophthalmoparesis (9/19 = 47.4%) vs GBS-

Table 2 Therapy and prognosis in GBS-AV(+) and GBS-AV(−) groups

Parameters	GBS-AV(+), n = 42	GBS-AV(−), n = 75	*p* Value
Treatment, no. (%)			
PE	15 (36)	12 (16)	0.03
IA	16 (38)	35 (47)	0.7
DFPP	12 (29)	15 (20)	0.6
IVIG	11 (26)	4 (5.3)	0.004
Combination therapy	11 (26)	7 (9.3)	0.03
Prognosis,* no. (n)			
1 mo	35† (37)‡	18 (28)	0.005
2 mo	23 (27)	10 (17)	0.1

* Scoring >2 on the Hughes Grading Scale (≧3).
† No. of patients scoring >2 on the Hughes Grading Scale 1 mo after disease onset.
‡ n = total no. of patients with available follow-up data.

GBS = Guillain–Barré syndrome; AV = artificial ventilation; PE = plasma exchange; IA = immunoadsorption; DFPP = double-filtered plasmapheresis; IVIG = IV immunoglobulin.

Table 3 Antiganglioside antibody frequency

	GBS-AV(+), n = 44	GBS-AV(−), n = 87	*p* value*	Odds ratio
Antibody positive, no. (%)	25 (57)	54 (62)	>0.9	
IgG class, no. (%)				
Anti-GM1	4 (9)	19 (22)	0.11	
Anti-GM2	0 (0)	0 (0)		
Anti-GM3	0 (0)	0 (0)		
Anti-GD1a	6 (14)	4 (5)	0.13	
Anti-GalNAc-GD1a	3 (7)	13 (15)	0.36	
Anti-GD1b	9 (20)	14 (16)	0.7	
Anti-GD3	2 (5)	1 (1)	0.44	
Anti-GT1b	3 (7)	2 (2)	0.4	
Anti-GQ1b	12 (27)	7 (8)	0.006	4.29
Anti-GM1b	2 (5)	3 (3)	>0.9	
Anti-GT1a	11 (31)*	11 (13)†	0.04	2.96
IgM class, no. (%)				
Anti-GM1	4 (9)	13 (15)	0.51	
Anti-GM2	1 (2)	7 (8)	0.36	
Anti-GM3	0 (0)	0 (0)		
Anti-GD1a	1 (2)	0 (0)	0.67	
Anti-GalNAc-GD1a	2 (5)	9 (10)	0.43	
Anti-GD1b	1 (2)	3 (3)	>0.9	
Anti-GD3	0 (0)	1 (1)	>0.9	
Anti-GT1b	1 (2)	0 (0)	0.67	
Anti-GQ1b	2 (5)	3 (3)	>0.9	
Anti-GM1b	1 (2)	2 (2)	>0.9	
Anti-GT1a	NS	NS		

* n = 35.
† n = 82.

GBS = Guillain–Barré syndrome; AV = artificial ventilation; NS = not studied.

AV(−) with ophthalmoparesis (7/15 = 46.7%; $p > 0.9$, χ^2 test), GBS-AV(+) without ophthalmoparesis (2/25 = 8.0%) vs GBS-AV(−) without ophthalmoparesis (4/67 = 6.3%; $p > 0.9$, Fisher exact probability). A multiple logistic regression model identified only IgG anti-GQ1b antibody as an independent variable correlated with artificial ventilation ($p = 0.04$, odds ratio 7.23).

Discussion. Our findings show that multiple cranial nerve involvement and the presence of IgG anti-GQ1b antibody are important factors predictive of respiratory muscle weakness in GBS. Multiple logistic testing may obscure statistical correlation when variables are not appropriately selected. We selected eight IgG antiganglioside antibodies as individual variables in view of the validity of a multiple logistic regression model. Although pure pharyngeal palsy without respiratory muscle weakness can be an important indication for artificial ventilation, all ventilated patients in our study had respiratory muscle weakness with or without pharyngeal palsy. Bulbar and facial palsies have been reported to be predictive features of respiratory muscle weakness in GBS.[1] An overlap of lower cranial nerve involvement, ophthalmoplegia, and facial diplegia is common in GBS.[7] Our results are consistent with these reports. Certain muscle groups (extraocular, levator, pharyngeal, neck, and respiratory muscles) are preferentially involved in such neuromuscular transmission disorders as myasthenia gravis and botulism. The inference based on clinical features is that neuromuscular junction (NMJ) involvement may contribute to oculomotor, facial, and respiratory muscle weakness in ventilated patients with GBS.

This inference is supported by our findings that the presence of anti-GQ1b antibody is associated with respiratory muscle weakness. In vitro electrophysiologic and morphologic studies show that human and mouse anti-GQ1b antibodies have an α-latrotoxin (LTx)–like blockade effect on neuromuscular transmission.[8] Moreover, passive transfer of sera from botulism or Miller–Fisher syndrome (MFS) patients produced respiratory muscle weakness in mice.[9] In GBS patients with respiratory paresis, the motor nerve terminals of the respiratory muscle may be a candidate for the target of anti-GQ1b antibodies. Because few MFS patients have respiratory paresis, respiratory muscle weakness cannot be explained by the presence of anti-GQ1b antibody alone. Infrequency of respiratory failure in MFS may be associated with differences in the vulnerability to and thresholds of the α-LTx-like effect of anti-GQ1b antibodies in the NMJ of various muscle groups, in addition to the fine specificity of anti-GQ1b antibody. On the other hand, the specific binding of anti-GQ1b IgG antibodies to the paranodal myelin of the oculomotor, trochlear, and abducens nerves may account for the exceptionally high occurrence of ophthalmoplegia in patients with anti-GQ1b IgG antibodies.[10]

Frequency of ventilated patients with GBS and their mortality rate in our series were lower than those in previous reports,[1,2] which might result from advances in supportive care and the recent widespread use of specific treatments such as plasmapheresis and IV immunoglobulin therapy.

Thus, the presence of IgG anti-GQ1b antibody may be a factor predictive of respiratory failure. Development of a more rapid and easier assay system of antiganglioside antibodies is desired for practical use.

Acknowledgment

The authors thank the attendant physicians at the following universities and hospitals for the data collection: Universities: Gunma, Jichi-ika, Jikei-ika, Kagoshima, Kyushu, Nihon-ika, Osaka-ichiritsu, Tottori. Hospitals: Bokuto, Iizuka, Japan Red Cross, Kagoshimashi-Ishikai, Konan, Koritsu-Showa, Kumamotoshimin, Maebashi Red Cross, NTT-Kanto, Shakaihoken-Chukyo, Toranomon. They also thank Dr. Kazuo Yamakawa (Juntendo-Urayasu Hospital) for re-collection of clinical data, Ms. Miwako Suemura (National Defense Medical College) for measuring anti-GT1a antibody activities by ELISA, and Dr. Hiroshi Ashida (Division of Biomedical Information Sciences, National Defense

Medical College Research Institute) for useful advice on the statistical analyses.

References

1. Fletcher DD, Lawn ND, Wolter TD, Wijdicks EFM. Long-term outcome in patients with Guillain–Barré syndrome requiring mechanical ventilation. Neurology 2000;54:2311–2315.
2. Lawn ND, Fletcher DD, Henderson RD, Wolter TD, Wijdicks EFM. Anticipating mechanical ventilation in Guillain–Barré syndrome. Arch Neurol 2001;58:893–898.
3. Willison HJ, Yuki N. Peripheral neuropathies and anti-glycolipid antibodies. Brain 2002;125:2591–2625.
4. Asbury AK, Cornblath DR. Assessment of current diagnostic criteria for Guillain–Barré syndrome. Ann Neurol 1990;27(suppl):S21–S24.
5. Hughes R, Newsom–Davis J, Perkin G, Pierce J. Controlled trial of prednisolone in acute polyneuropathy. Lancet 1978;2:750–753.
6. Kaida K, Kusunoki S, Kamakura K, Motoyoshi K, Kanazawa I. Guillain–Barré syndrome with antibody to a ganglioside, *N*-acetylgalactosaminyl GD1a. Brain 2000;123:116–124.
7. ter Bruggen JP, van der Meché FGA, de Jager AEJ, Polman CH. Ophthalmoplegic and lower cranial nerve variants merge into each other and into classical Guillain–Barré syndrome. Muscle Nerve 1998;21: 239–242.
8. O'Hanlon GM, Plomp JJ, Chakrabarti M, et al. Anti-GQ1b ganglioside antibodies mediate complement-dependent destruction of the motor nerve terminal. Brain 2001;124:893–906.
9. Notermans SHW, Wokke JHJ, van den Berg LH. Botulism and Guillain–Barré syndrome. Lancet 1992;340:303.
10. Chiba A, Kusunoki S, Obata H, Machinami R, Kanazawa I. Serum anti-GQ1b IgG antibody is associated with ophthalmoplegia in Miller–Fisher syndrome and Guillain–Barré syndrome: clinical and immunohistochemical studies. Neurology 1993;43:1911–1917.

RESEARCH COMMUNICATION

Primitive neural stem cells from the mammalian epiblast differentiate to definitive neural stem cells under the control of Notch signaling

Seiji Hitoshi,[1,2,3,4] Raewyn M. Seaberg,[2] Cheryl Koscik,[2] Tania Alexson,[2] Susumu Kusunoki,[1] Ichiro Kanazawa,[1] Shoji Tsuji,[1] and Derek van der Kooy[2,5]

[1]Department of Neurology, University of Tokyo, Tokyo 113-8655, Japan; [2]Department of Medical Genetics and Microbiology, University of Toronto, Toronto, Ontario M5S 1A8, Canada

Basic fibroblast growth factor (FGF2)-responsive definitive neural stem cells first appear in embryonic day 8.5 (E8.5) mouse embryos, but not in earlier embryos, although neural tissue exists at E7.5. Here, we demonstrate that leukemia inhibitory factor-dependent (but not FGF2-dependent) sphere-forming cells are present in the earlier (E5.5–E7.5) mouse embryo. The resultant clonal sphere cells possess self-renewal capacity and neural multipotentiality, cardinal features of the neural stem cell. However, they also retain some nonneural properties, suggesting that they are the in vivo cells' equivalent of the primitive neural stem cells that form in vitro from embryonic stem cells. The generation of the in vivo primitive neural stem cell was independent of Notch signaling, but the activation of the Notch pathway was important for the transition from the primitive to full definitive neural stem cell properties and for the maintenance of the definitive neural stem cell state.

Received March 31, 2004; revised version accepted May 26, 2004.

The epiblast is endowed with positional information along its anteroposterior axis by the primitive streak stage at embryonic day 6.5 (E6.5), and the anteromedial part of the epiblast is further specified to form neural plate by E7.5 in the mouse embryo. Expression of neural tissue-specific marker genes, such as *Nestin* and *Sox1*, first becomes detectable at E7.0–E8.0 (Wood and Episkopou 1999; Kawaguchi et al. 2001). This happens before the first appearance of basic fibroblast growth factor (FGF2)-responsive neural stem cells at E8.5 (Tropepe et al. 1999). Thus, the first neurally specified cell in the epiblast could be a transient neural progenitor cell that is induced (by signals from mesoderm or endoderm) to yield neural stem cells, or perhaps, more interestingly, a primitive neural stem cell itself that builds the neural plate before giving rise to the definitive neural stem cell. Here, we define the "definitive" neural stem cell as the neural stem cell that is present in the late embryonic or adult brain and proliferates in response to FGF2 (and epidermal growth factor [EGF], or has the potential to acquire EGF responsiveness) to form clonal floating sphere colonies in vitro.

We developed a colony-forming ES sphere assay, in which embryonic stem (ES) cells are cultured in serum-free media in the presence of leukemia inhibitory factor (LIF; at clonal density or as single cells) to generate nestin$^+$ floating sphere colonies (ES spheres; Tropepe et al. 2001). The ES sphere-forming cells show the cardinal features of neural stem cells, self-renewal and neural multipotentiality, but also possess some pluripotency in generating nonneural progeny, and hence were termed primitive neural stem cells (Tropepe et al. 2001). We suggest that in the absence of positive or negative instructive signals, primitive neural stem cells default from ES cells. Although some endogenous signals (e.g., FGF2) may be in fact indispensable for neural induction, survival, or proliferation, these signals may be concealed by autocrine mechanisms (Streit et al. 2000; Tropepe et al. 2001; Wilson and Edlund 2001; Ying et al. 2003). We hypothesize that epiblast cells are inhibited by endogenous factors (e.g., bone morphogenetic proteins [BMPs]) until definitive neural stem cells are created, as this inhibition is relieved when the neural tube forms later in embryogenesis. This hypothesis predicts that primitive neural stem cells can be isolated from the early mouse embryo prior to E7.5 in vivo.

Historically, Notch signaling in *Drosophila* was thought to maintain cells in an undifferentiated state through a lateral inhibition mechanism (Artavanis-Tsakonas et al. 1995; Kimble and Simpson 1997). The Notch signaling also plays significant roles in mammalian neurogenesis: disruption of Notch pathway genes results in the reduction of the neural stem cell pool size (Nakamura et al. 2000; Hitoshi et al. 2002). The activation of this signaling promotes the symmetrical divisions of neural stem cells, and thereby enhances the self-renewal ability of the neural stem cells. However, little is known about molecular mechanisms underlying the generation of primitive and definitive neural stem cells in vivo. In this study, we used an in vitro colony-forming sphere assay to isolate primitive neural stem cells from early mouse embryos and demonstrated a role for Notch signaling in the generation of definitive neural stem cells.

Results and Discussion

Mouse E7.5 neuroectoderm was dissociated to single cells and cultured in serum-free media containing LIF to clonally generate nestin$^+$ floating sphere colonies (Fig. 1A). When dissociated cells from E7.5 CD1 and from green fluorescent protein (GFP)-expressing neuroectoderm were equally mixed (at a final density of 10 cells/μL) and then proliferated to form LIF-dependent spheres, spheres containing both GFP$^+$ and GFP$^-$ cells never were observed (Fig. 1A), suggesting that the primary LIF-dependent spheres were clonally derived from single cells.

[*Keywords*: Neural stem cell; embryonic stem cell; epiblast; neuroectoderm; leukemia inhibitory factor; Notch signaling]
[3]**Present address: Division of Neurobiology & Bioinformatics, National Institute for Physiological Sciences, Aichi 444-8585, Japan.**
Corresponding authors.
[4]**E-MAIL shitoshi@nips.ac.jp; FAX 81-564-59-5247.**
[5]**E-MAIL derek.van.der.kooy@utoronto.ca; FAX (416) 978-3844.**
Article and publication are at http://www.genesdev.org/cgi/doi/10.1101/gad.1208404.

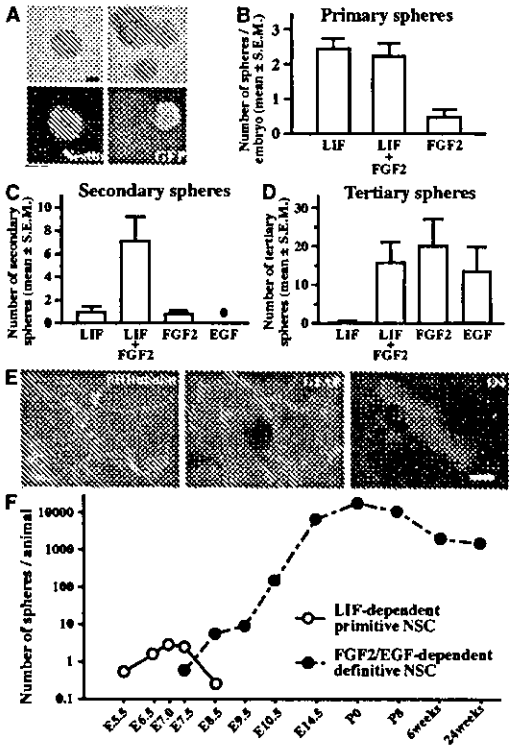

Figure 1. LIF-dependent primitive neural stem cell spheres. (*A*) The spheres (*top left*) generated from the E7.5 mouse neuroectoderm were immunopositive for nestin (*bottom left*). Dissociated E7.5 neuroectoderm cells from CD1 embryos and from GFP mouse embryos were mixed in equivalent proportions (to a final cell density of 10 cells/μL) and proliferated to form LIF-dependent spheres (*top right*). The complete lack of GFP$^+$ cells in the white spheres (*bottom right*) shows that the spheres were clonally derived from single cells. Bar, 0.1 mm. (*B*) The average sphere numbers in the presence of LIF (n = 32 embryos), FGF2 (n = 16 embryos), or both (n = 35 embryos) per embryo are shown. (*C*) Single primary LIF-dependent spheres produced secondary spheres in the presence of both LIF and FGF2 (n = 10 or more). (*D*) Single secondary spheres cultured in both LIF and FGF2 responded to either FGF2 or EGF to produce tertiary spheres (n = 16 or more). (*E*) The primary and passaged E7.5 sphere contained cells that could differentiate into βIII tubulin$^+$ neurons, GFAP$^+$ astrocytes, or O4$^+$ oligodendrocytes in vitro. Bar, 40 μm. (*F*) The average numbers of LIF-dependent spheres (open circles) and FGF2/EGF-dependent forebrain neurospheres (closed circles) per animal that were isolated at different times throughout development and into the adult mouse are plotted.

At E7.5, very few spheres formed in the media containing only FGF2, and adding FGF2 did not significantly increase the numbers that formed in LIF alone (Fig. 1B). However, FGF2 secreted from the primary LIF-dependent cells themselves (Fig. 2A) may suffice for transducing the FGF2 signal through autocrine or paracrine mechanisms, leaving open the possibility that the activation of FGF signaling is necessary for the formation of spheres from E7.5 neuroectoderm.

Self-renewal and neural multilineage potential are hallmark features of neural stem cells. The primary E7.5 primitive neural stem cell spheres cultured in LIF were capable of producing secondary spheres after dissociation in the presence of both LIF and FGF2, but only very poorly in the presence of LIF alone or FGF2 alone (Fig. 1C). No secondary spheres were found in EGF alone. However, the secondary spheres cultured in both LIF and FGF2 could be dissociated again to produce clonal tertiary spheres in the presence of either FGF2 alone or EGF alone (Fig. 1D). These neural stem cells then could be maintained and passaged in either of the same media. In vivo, EGF-dependent neural stem cells start to descend from their earlier FGF2-dependent ancestor neural stem cells (Tropepe et al. 1999), and the sequence and time course of their lineage appears to be maintained in vitro by the primitive neural stem cells isolated from the E5.5–E7.5 embryo. Cells from the primary LIF-dependent as well as passaged FGF2- or EGF-dependent sphere could differentiate into neurons, astrocytes, or oligodendrocytes in vitro (Fig. 1E), demonstrating that the LIF-dependent primitive neural stem cells (and then their in vitro definitive FGF2- and EGF-dependent neural stem cell progeny) were multipotent in the neural lineage. These observations suggest that the primitive, LIF-dependent neural stem cells derived from E5.5–E7.5 embryos in vivo have a capacity to self-renew and also show neural multipotentiality as definitive neural stem cells.

To exclude the possible involvement of mesenchymal cells in sphere formation, we dissected earlier embryos before the migration of mesodermal tissue beneath the anterior neuroectoderm. LIF-dependent spheres could be isolated from the epiblast at the prestreak stage (E6.5) or even at the egg cylinder stage (E5.5; Fig. 1F). During the E7.5–E8.5 period, LIF-dependent sphere-forming neural stem cells diminished and were replaced by the emergence of FGF2-dependent definitive neural stem cells (Fig. 1F). These results parallel the emergence from ES cells in vitro of LIF-dependent, clonal primitive neural stem cell spheres, which then give rise directly to clonal FGF2-dependent spheres in vitro (Tropepe et al. 2001). Thus, LIF-dependent primitive neural stem cells are present in the epiblast/neuroectoderm of E5.5–E7.5 mouse embryo. These primitive neural stem cells emerge independent of mesodermal influence in vivo, although these experiments do not rule out a possible role for visceral endoderm effects in vivo.

ES-derived primitive neural stem cell spheres express some nonneural marker genes such as *GATA4* (an early primitive and definitive endodermal marker; Tropepe et al. 2001), in addition to neural precursor markers such as *FGF5* and *Sox2* and a neural marker *Sox1* (Fig. 2B). *FGF5* is expressed in primitive ectoderm but down-regulated after E7.5 in the mouse embryo (Hébert et al. 1991), whereas *Sox1* expression is first detectable in the neural plate at E7.5 of the mouse embryo, and *Sox2* is expressed earlier in the epiblast (Wood and Episkopou 1999). These gene expression properties of ES cell-derived spheres are unaltered after repeated passaging procedures (Fig. 2B). RT–PCR was used to analyze marker gene expression in the primary LIF-dependent and passaged EGF-dependent spheres from the E6.5 mouse epiblast, a time when mesoderm does not underlie the anterior epiblast. Primary E6.5 epiblast-derived spheres showed a gene expression pattern very similar to that of ES spheres; they expressed *GATA4*, *FGF5*, *Sox2*, and *Sox1* (Fig. 2B), but did not express *Brachyury* (a mesodermal marker), *HNF4* (a mature endodermal marker), or *cytokeratin17* (a epidermal marker). In contrast, E6.5 spheres that were passaged in EGF down-regulated *GATA4* and *FGF5* expression and presented a similar gene expression pattern to that of definitive neural stem cell neurospheres isolated from the later embryonic brain (Fig. 2B). These results suggest that epiblast-derived LIF-dependent spheres arise from

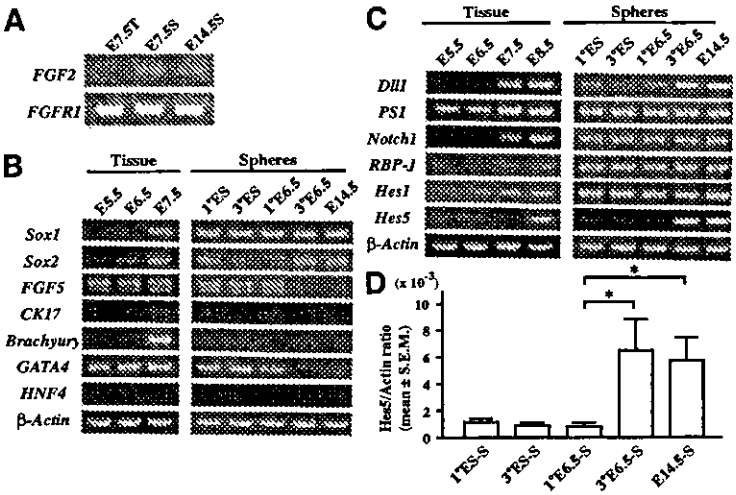

Figure 2. Gene expression profiles of the primary tissue and clonal spheres. (*A*) Primary E7.5 neuroectoderm-derived spheres (E7.5S), tissue (E7.5T) from which the sphere derived, and E14.5 definitive neural stem cell neurospheres (E14.5S) were analyzed by RT–PCR for the expression of *FGF2* and *FGF receptor 1* (FGFR1). (*B,C*) Primary and tertiary E6.5 epiblast-derived spheres (1° and 3° E6.5), as well as ES-derived primitive neural stem cell spheres (1° and 3° ES) and primary E14.5 definitive neural stem cell spheres (E14.5) were analyzed by RT–PCR. (*D*) The amounts of *Hes5* gene mRNA were quantified by real time RT–PCR using the LightCycler system. The ratios of *Hes5* mRNA copy numbers to those of β-*actin* are shown. Data represent means ± S.E.M. (*) $P < 0.05$.

the proliferation of a neural stem cell equivalent to the ES cell-derived primitive neural stem cells. However, the in vivo E6.5 primitive neural stem cells differentiate in vitro into neural stem cells that are similar to those derived from the forebrains of late embryos or adult mice, unlike the ES-derived primitive neural stem cells whose gene expression profiles do not mature to resemble definitive neural stem cells and do not produce EGF-responsive definitive neural stem cells.

Notch signaling is essential for the maintenance of the neural stem cell, by enhancing the self-renewal of the neural stem cell and by inhibiting its differentiation into neuronal and glial progenitors (Nakamura et al. 2000; Hitoshi et al. 2002). The generation of primary ES spheres in vitro was unaltered in ES cells deficient for the common Notch downstream signaling factor RBP-J (Hitoshi et al. 2002), suggesting that the formation of primitive neural stem cells is independent of Notch activity. However, the role of Notch signaling on the generation of primitive neural stem cells in vivo remains unknown. Expression profiles for Notch pathway genes from the tissues of early embryos, from which spheres were generated, and from the clonal epiblast spheres themselves, were analyzed by RT–PCR (Fig. 2C). Notch activation was assessed by the extent to which *Hes5*, one of the downstream target genes of Notch signaling, was expressed (de la Pompa et al. 1997; Donoviel et al. 1999; Handler et al. 2000). *Hes5* expression was first detected in the neuroepithelium at E8.5, when definitive FGF2-dependent neural stem cells first appear in vivo. The other molecules in the Notch pathway were expressed stably in the primary and passaged ES-derived and E6.5 epiblast-derived primitive neural stem cell spheres, as well as in E14.5 definitive neural stem cell neurospheres (Fig. 2C). However, *Hes5* expression (assessed by quantitative RT–PCR) in the LIF-dependent, primary E6.5 spheres, as well as in the primary ES spheres, was much weaker (and sometimes below detectable levels) compared with the substantial expression in E14.5 definitive neurospheres (Fig. 2C,D). After passaging in vitro, FGF2- or EGF-responsive tertiary E6.5 spheres up-regulated the *Hes5* gene to an extent similar to that observed in the E14.5 brain-derived neurospheres. In contrast, passaged ES spheres (which self-renew in the presence of LIF and FGF2 but never in the presence of EGF) continued to express only weakly (if at all) the *Hes5* gene (Fig. 2C,D). These results suggest that Notch signaling is activated strongly during the transition from primitive to definitive neural stem cells in vitro and in vivo.

The in vivo roles of Notch signaling in the generation of primitive and definitive neural stem cells were further investigated using mouse embryos deficient for Notch1 (Conlon et al. 1995). Comparable numbers of LIF-dependent primitive neural stem cells were present in the neural plate of E7.5 *Notch1*$^{-/-}$ embryos and their littermate controls (Fig. 3A). The primary LIF-dependent spheres from E7.5 *Notch1*$^{-/-}$ embryos expressed less *Hes5* than their littermate controls (Fig. 3B), but still retained neural multipotentiality (Fig. 3C). On the other hand, the FGF2-responsive definitive neural stem cells in the E8.0 *Notch1*$^{-/-}$ embryos were significantly lower in number than those in their littermate controls (Fig. 3D). This decrement was not due to a delayed transition in the *Notch1*$^{-/-}$ embryos from primitive to definitive neural stem cells, because LIF-dependent primitive neural stem cell numbers decreased similarly between E7.5 and E8.0 in *Notch1*$^{-/-}$ and control embryos (Fig. 3A). The number of tertiary EGF-responsive definitive neural stem cells generated by passaging primary E7.5 LIF-dependent primitive neural stem cell spheres in vitro was reduced greatly in *Notch1*$^{-/-}$ embryos compared with their littermate controls (Fig. 3E). Thus, the *Notch1* mutation impaired the transition from the primitive to definitive neural stem cells not only in vivo (Fig. 3A,D), but also in vitro (Fig. 3E).

These observations prompted us to ask if Notch activation promotes the transition from the LIF-dependent ES cell-derived primitive neural stem cell to the EGF-dependent neural stem cell. ES cell-derived spheres, which can be maintained continuously in LIF and FGF2 media but not in EGF media, were infected with retrovirus expressing constitutively active Notch1 or control retrovirus (both express enhanced GFP as a reporter; Fig. 4A), and then cultured in LIF and FGF2 media to generate secondary ES spheres. The resultant individual secondary ES spheres showed variable GFP expression patterns, because infection and retroviral gene integration may occur at different times during sphere formation. Strongly GFP$^+$ secondary ES spheres were selected under a fluorescent microscope and passaged to yield tertiary ES spheres in LIF and FGF2 or in EGF alone. Significant numbers of EGF-responsive tertiary ES spheres were observed only after infection with active Notch1 retrovirus (Fig. 4B), whereas very few EGF-responsive tertiary ES spheres were found after control retrovirus infection. The numbers of tertiary ES spheres grown in both LIF

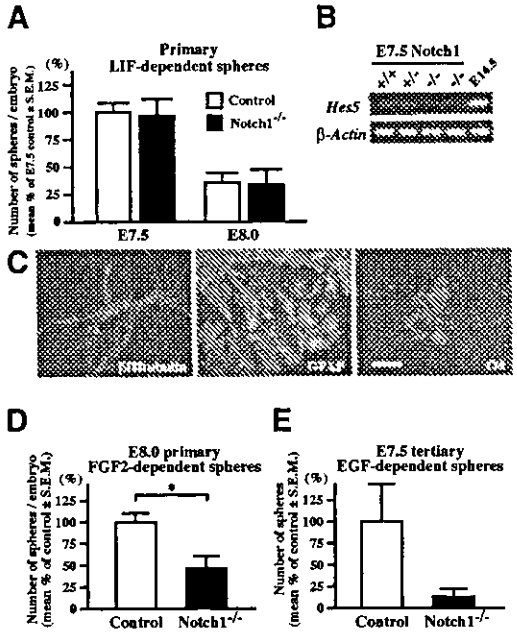

Figure 3. The formation of neural stem cell spheres from Notch1 mutant embryos. (*A*) The numbers of primary LIF-dependent spheres from E7.5 and E8.0 *Notch1*$^{-/-}$ embryos (n = 7 at E7.5 and n = 6 at E8.0) and littermate controls (n = 18 at E7.5 and n = 25 at E8.0) are shown. (*B*) The expression of *Hes5* was abolished in the primary E7.5 *Notch1*$^{-/-}$ spheres. (*C*) The primary E7.5 *Notch1*$^{-/-}$ spheres retained multipotentiality within the neural lineage. Bar, 50 μm. (*D*) The numbers of primary FGF2-dependent neurospheres from E8.0 *Notch1*$^{-/-}$ embryos (n = 19) and littermate controls (n = 57). (*) $P < 0.05$. (*E*) The primary LIF-dependent spheres from each E7.5 *Notch1*$^{-/-}$ (n = 7) and littermate control (n = 18) embryo were separately passaged twice in vitro to generate tertiary EGF-dependent neurospheres. The numbers of EGF-dependent tertiary neurospheres from each embryo are shown.

and FGF2 were comparable between the ES spheres infected with active Notch1 and with control retrovirus, demonstrating that cell numbers plated and viability of the cells were comparable between both groups. Notch signaling was activated, as assessed by the greater amounts of *Hes5* gene expression in the tertiary EGF-responsive spheres infected with the active Notch1 retrovirus than in similar spheres infected with the control retrovirus (Fig. 4C). These results demonstrated that activation of the Notch pathway promotes the emergence of EGF-responsive spheres from LIF-dependent ES spheres. Thus, both in vivo data using the *Notch1*$^{-/-}$ embryos and in vitro experiments using the ES cell-derived spheres suggest that Notch activation is important for the transition from the LIF-dependent primitive neural stem cell to the EGF-dependent definitive neural stem cell and for the maintenance of the definitive neural stem cell state.

Early experiments using animal cap explants (that are uncommitted ectoderm and normally give rise to epidermis) from *Xenopus* blastula-stage embryos revealed that after dissociation at low density, the cells became neural tissue (Godsave and Slack 1989; Grunz and Tacke 1989; Sato and Sargent 1989). Later, this fating to neural cells was shown to be accomplished by the inhibition of TGF-β activity (Smith et al. 1993; Hemmati-Brivanlou and Melton 1994; Sasai et al. 1995), leading to the proposal that neural fate specification from uncommitted blastocyst tissue occurs by a default mechanism. We have shown that this default model may be applicable to mammalian neural induction by demonstrating that mouse ES cells cultured at low cell density (or even as single cells) in serum-free media took on neural identities after 4 h (Tropepe et al. 2001). In the presence of LIF, a small percentage of the ES cells that may default to a neural state proliferated as primitive neural stem cells in vitro (Tropepe et al. 2001). We suggest that in vivo, where cell density and cell-to-cell interactions are high, pluripotent inner cell mass and epiblast cells receive dense signals that inhibit neural induction and the cells may acquire minimal neural identities as primitive neural stem cells (or at least as potential primitive neural stem cells in vivo), until neural inhibition is fully suppressed by TGF-β family antagonists at E7.5–E8.5 when definitive neural stem cells are formed.

Only a few cells that reside in the anterior part of E7.5 neuroectoderm formed clonal primitive neural stem cell spheres (~0.1%). The isolation of only rare primitive neural stem cells might be explained in three ways. First, most (if not all) of the putative neuroectodermal cells possess the potential to respond to LIF to proliferate and form spheres, but many may be unable to survive the trituration and serum-free culture conditions. Second, only a few specific cells among all of the putative neuroectoderm cells retain (or can take on) a neural stem cell fate. It would be intriguing to use factors that enhance the survival of (primitive) neural stem cells in the serum-free sphere assay. Indeed, we have found some survival factors increase the cell viability of ES-derived neural cells so that much higher frequencies of spheres are formed (Smukler et al. 2003). However, these same survival factors appear not to increase the frequency of isolating primitive neural stem cells from the epiblast (S. Hitoshi, unpubl.), suggesting that only a few epiblast/early neuroectoderm cells may have the potential to be

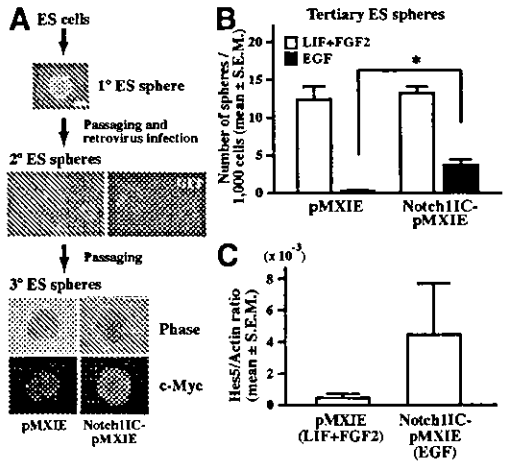

Figure 4. Active Notch1 retrovirus infection of ES spheres. (*A*) A schema of the experimental procedures. Some of secondary spheres infected with the retrovirus showed GFP$^+$ expression. After passaging, tertiary spheres infected with pMXIE-Notch1IC were homogenously positive for c-Myc that is tagged to Notch1IC. Bar, 0.1 mm. (*B*) The numbers of tertiary spheres generated in both LIF and FGF2 and in EGF-only media are shown. Data represent means ± S.E.M. from three independent experiments. (*) $P < 0.05$. (*C*) The amounts of *Hes5* gene expression were quantified (n = 3).

primitive neural stem cells. Third, the rarity of primitive neural stem cells in the epiblast/neuroectoderm might derive from the presence of a few pluripotent ES cells that remain until E7.5 of mouse development. However, this third possibility seems unlikely because ES cells never have been isolated from mouse embryos after the egg cylinder stages (Smith 2001) and because the number of sphere-forming primitive neural stem cells increased during E5.5–E7.0 in the epiblast/neuroectoderm (present study).

In the mouse embryo deficient for Notch pathway molecules, the size of the definitive neural stem cell pool is reduced (Nakamura et al. 2000; Hitoshi et al. 2002). Activation of Notch signaling is indispensable for maintaining the neural stem cell by enhancing its self-renewal capacity and by repressing differentiation into progenitor cells (Fig. 5; Hitoshi et al. 2002). The current results suggest an additional role for Notch signaling in neural stem cell ontogenesis; activation of Notch pathway is required for the transition from the primitive neural stem cell to the definitive neural stem cell, which subsequently acquires EGF responsiveness. The reduction of definitive neural stem cells observed in E8.0 *Notch1*$^{-/-}$ embryos in vivo, as well as the reduction seen in the EGF-responsive tertiary spheres from E7.5 *Notch1*$^{-/-}$ primitive neural stem cell spheres in vitro, are consistent with this model. Certainly, the appearance of some definitive neural stem cells in the E7.5 *Notch*$^{-/-}$ embryos suggests that other signaling pathways may permit some transition from primitive to definitive neural stem cells. However, another model also is possible: definitive neural stem cells are generated from the primitive neural stem cells independent of Notch signaling, but definitive neural stem cells may require Notch signaling for their maintenance, as suggested previously (Hitoshi et al. 2002). These two possibilities are not mutually exclusive and current data do not allow us to discriminate between them. Later in development, Notch signaling may play additional roles in enhancing the symmetric and self-renewing divisions of definitive neural stem cells and suppressing asymmetric division of neural stem cells to produce neuronal and glial progenitor cells (Hitoshi et al. 2002). This later function appears inconsistent with the recent notion of an instructive role for Notch signaling to produce glia from neural progenitor cells in the mammalian central nervous system (Gaiano et al. 2000). However, this inconsistency disappears if adult forebrain neural stem cells acquire some glial features (but do not differentiate into unipotential glial cells), as suggested by demonstrations that Notch signaling enhances GFAP transcription in adult neural progenitor cells (Tanigaki et al. 2001) and that at least some of the GFAP-expressing astrocytes in the adult forebrain subependyma are, indeed, neural stem cells (Doetsch et al. 1999; Morshead et al. 2003).

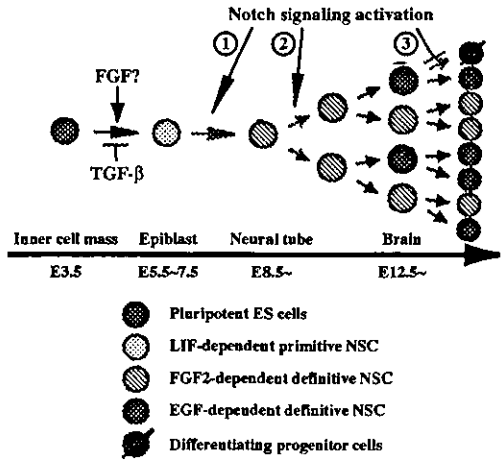

Figure 5. A model of neural stem cell development. LIF-dependent primitive neural stem cells can be generated directly from single ES cell in vitro after relieving TGF-β inhibition (Tropepe et al. 2001) and now have been shown to exist (at least potentially in vivo and literally in vitro) in the E5.5–E7.5 epiblast/neuroectoderm of mouse embryos. Whether or not FGF signaling promotes the induction of primitive neural stem cells in vivo (or just their survival or proliferation) remains to be determined. Activation of the Notch pathway could be required for the transition from primitive to definitive neural stem cells that autonomously acquire EGF responsiveness (①) and/or for the maintenance of definitive, FGF2- or EGF-dependent neural stem cells by enhancing their self-renewal (②) and thus suppressing their differentiation into neuronal or glial unipotential progenitors (③).

Materials and methods

Animals and cell culture

CD1 mice (Charles River) were used in this study. The generation and genotyping of *Notch1* mutant mice (Conlon et al. 1995) and GFP transgenic mice (Hadjantonakis et al. 1998) on a CD1 background have been described. Midday of the plugged day was termed E0.5 and the staging of the early embryos followed (Downs and Davies 1993). Prospective head regions from E7.5 mouse embryos at late primitive streak stage or at early headfold stage, or from E8.0–E8.5 embryos at late headfold stage but before turning were excised and treated with papain (1 unit/mL, Worthington) in phosphate-buffered saline containing 0.2 mg/mL cysteine, 5 mg/mL glucose, and 0.4 mg/mL bovine serum albumin for 4 min. Neuroepithelium was detached from underlying tissue and triturated into single cells. Usually, 2000–3000 viable cells were collected from each E7.5 embryo. The cells were cultured in serum-free media (Tropepe et al. 1999) containing LIF (1×10^3 units/mL, Chemicon) and B27 supplement (Invitrogen). The cells from each embryo at E7.5 or E8.0 were cultured in 24-well (0.5 mL/well) plates, where usual cell densities were below 10 cells/μL. The anterior parts of the E6.5–E7.0 embryos at the early primitive streak stage were excised, triturated into single cells, and cultured as described earlier. Distal portions of the E5.5–E6.5 embryos at the egg cylinder stage or at the preprimitive streak stage were also excised, roughly triturated leaving small clumps, and then cultured as described earlier. The dissection and cell culture of forebrains from mouse embryos at and after E8.5 or adult mice, the passaging procedures, differentiation assay, and immunohistochemical analysis procedures also have been described (Tropepe et al. 1999; Hitoshi et al. 2002).

Immunocytochemistry

Immunocytochemical analyses were performed as described previously (Hitoshi et al. 2002). We used anti-nestin mouse monoclonal (IgG; 1:100; Chemicon), anti-βIII tubulin mouse monoclonal (IgG; 1:200; Sigma), anti-GFAP rabbit polyclonal (IgG; 1:400; Chemicon), anti-O4 mouse monoclonal (IgM; 1:40; Roche), or anti-c-Myc mouse monoclonal (IgG; 1:500; Santa Cruz) antibodies as primary, followed by appropriate FITC- or TRITC-conjugated secondary antibodies. Cultures were counterlabeled with the nuclear stain Hoechst 33258 (1 μg/mL; Sigma).

RT-PCR

cDNA synthesis, some of the primer sequences, and PCR cycling procedures have been described (Tropepe et al. 2001; Hitoshi et al. 2002). Primer sequences and PCR cycling conditions will be provided on request. Quantitative RT-PCR analyses for *Hes5* and β-*actin* were performed using the LightCycler system (Roche) and using the same procedures described previously (Takahashi et al. 2003).

Retrovirus infection

The construction of replication-incompetent retroviral vector, pMXIE and Notch1IC-pMXIE, retrovirus preparation, and infection procedures

have been described (Hitoshi et al. 2002). Primary ES spheres were dissociated, infected with retrovirus, and then cultured in LIF and FGF2 media to generate secondary ES spheres. The resultant individual secondary ES spheres showed variable GFP expression patterns, because infection and retroviral gene integration may occur at different times during sphere formation. Strongly GFP$^+$ secondary ES spheres were picked up under a fluorescent microscope and passaged to yield tertiary ES spheres.

Acknowledgments

We thank R. Conlon for the Notch1 mutant mice and J. Nye for N-terminal Myc epitope-tagged Notch1IC. This work was supported by grants from the Canadian Institutes of Health Research (D.v.d.K.), and Grants-in-Aid for Scientific Research on Priority Areas—Advanced Brain Science Project—from the Ministry of Education, Culture, Sports, Science and Technology of Japan (S.H.), "Research for the Future (RFTF)" of the Japan Society for the Promotion of Science (S.H.), and the Cell Science Foundation (S.H.).

The publication costs of this article were defrayed in part by payment of page charges. This article must therefore be hereby marked "advertisement" in accordance with 18 USC section 1734 solely to indicate this fact.

References

Artavanis-Tsakonas, S., Matsuno, K., and Fortini, M.E. 1995. Notch signaling. *Science* **268:** 225–232.

Conlon, R.A., Reaume, A.G., and Rossant, J. 1995. *Notch1* is required for the coordinate segmentation of somites. *Development* **121:** 1533–1545.

de la Pompa, J.L., Wakeham, A., Correia, K.M., Samper, E., Brown, S., Aguilera, R.J., Nakano, T., Honjo, T., Mak, T.W., Rossant, J., et al. 1997. Conservation of the Notch signalling pathway in mammalian neurogenesis. *Development* **124:** 1139–1148.

Doetsch, F., Caille, I., Lim, D.A., Garcia-Verdugo, J.M., and Alvarez-Buylla, A. 1999. Subventricular zone astrocytes are neural stem cells in the adult mammalian brain. *Cell* **97:** 703–716.

Donoviel, D.B., Hadjantonakis, A.-K., Ikeda, M., Zheng, H., St George Hyslop, P., and Bernstein, A. 1999. Mice lacking both presenilin genes exhibit early embryonic patterning defects. *Genes & Dev.* **13:** 2801–2810.

Downs, K.M. and Davies, T. 1993. Staging of gastrulating mouse embryos by morphological landmarks in the dissecting microscope. *Development* **118:** 1255–1266.

Gaiano, N., Nye, J.S., and Fishell, G. 2000. Radial glial identity is promoted by Notch1 signaling in the murine forebrain. *Neuron* **26:** 395–404.

Godsave, S.F. and Slack, J.M. 1989. Clonal analysis of mesoderm induction in *Xenopus laevis*. *Dev. Biol.* **134:** 486–490.

Grunz, H. and Tacke, L. 1989. Neural differentiation of *Xenopus laevis* ectoderm takes place after disaggregation and delayed reaggregation without inducer. *Cell Differ. Dev.* **28:** 211–217.

Hadjantonakis, A.-K., Gertsenstein, M., Ikawa, M., and Nagy, A. 1998. Generating green fluorescent mice by germline transmission of green fluorescent ES cells. *Mech. Dev.* **76:** 79–90.

Handler, M., Yang, X., and Shen, J. 2000. Presenilin-1 regulates neuronal differentiation during neurogenesis. *Development* **127:** 2593–2606.

Hébert, J.M., Boyle, M., and Martin G.R. 1991. mRNA localization studies suggest that murine FGF-5 plays a role in gastrulation. *Development* **112:** 407–415.

Hemmati-Brivanlou, A. and Melton, D.A. 1994. Inhibition of activin receptor signaling promotes neuralization in *Xenopus*. *Cell* **77:** 273–281.

Hitoshi, S., Alexson, T., Tropepe, V., Donoviel, D., Elia, A.J., Nye, J.S., Conlon, R.A., Mak, T.W., Bernstein, A., and van der Kooy, D. 2002. Notch pathway molecules are essential for the maintenance, but not the generation, of mammalian neural stem cells. *Genes & Dev.* **16:** 846–858.

Kawaguchi, A., Miyata, T., Sawamoto, K., Takashita, N., Murayama, A., Akamatsu, W., Ogawa, M., Okabe, M., Tano, Y., Goldman, S.A., et al. 2001. Nestin-EGFP transgenic mice: Visualization of the self-renewal and multipotency of CNS stem cells. *Mol. Cell. Neurosci.* **17:** 259–273.

Kimble, J. and Simpson, P. 1997. The LIN-12/Notch signaling pathway and its regulation. *Annu. Rev. Cell Dev. Biol.* **13:** 333–361.

Morshead, C.M., Garcia, A.D., Sofroniew, M.V., and van der Kooy, D. 2003. The ablation of glial fibrillary acidic protein-positive cells from the adult central nervous system results in the loss of forebrain neural stem cells but not retinal stem cells. *Eur. J. Neurosci.* **18:** 76–84.

Nakamura, Y., Sakakibara, S.-i., Miyata, T., Ogawa, M., Shimazaki, T., Weiss, S., Kageyama, R., and Okano, H. 2000. The bHLH gene *Hes1* as a repressor of the neuronal commitment of CNS stem cells. *J. Neurosci.* **20:** 283–293.

Sasai, Y., Lu, B., Steinbeisser, H., and De Robertis, E.M. 1995. Regulation of neural induction by the Chd and Bmp-4 antagonistic patterning signals in *Xenopus*. *Nature* **376:** 333–336.

Sato, S.M. and Sargent, T.D. 1989. Development of neural inducing capacity in dissociated *Xenopus* embryos. *Dev. Biol.* **134:** 263–266.

Smith, A. 2001. Embryonic stem cells. In *Stem cell biology* (eds. D.R. Marshak, R.L. Gardner, and D. Gottlieb), pp. 205–230. Cold Spring Harbor Laboratory Press, Cold Spring Harbor, NY.

Smith, W.C., Knecht, A.K., Wu, M., and Harland, R.M. 1993. Secreted noggin protein mimics the Spemann organizer in dorsalizing *Xenopus* mesoderm. *Nature* **361:** 547–549.

Smukler, S.R., Xu, S., and van der Kooy, D. 2003. Enhanced ES-derived neurosphere formation with increased cell viability supports a model of default differentiation of ES cells into primitive neural stem cells. *Abstr. Soc. Neurosci.* 124.6.

Streit, A., Berliner, A., Papanayotou, C., Sirulnik, A., and Stern, C.D. 2000. Initiation of neural induction by FGF signalling before gastrulation. *Nature* **406:** 74–78.

Takahashi, Y., Jeong, S.Y., Ogata, K., Goto, J., Hashida, H., Isahara, K., Uchiyama, Y., and Kanazawa, I. 2003. Human skeletal muscle calcium channel α1S is expressed in the basal ganglia: Distinctive expression pattern among L-type Ca^{2+} channels. *Neurosci. Res.* **45:** 129–137.

Tanigaki, K., Nogaki, F., Takahashi, J., Tashiro, K., Kurooka, H., and Honjo, T. 2001. Notch1 and Notch3 instructively restrict bFGF-responsive multipotent neural progenitor cells to an astroglial fate. *Neuron* **29:** 45–55.

Tropepe, V., Sibilia, M., Ciruna, B.G., Rossant, J., Wagner, E.F., and van der Kooy, D. 1999. Distinct neural stem cells proliferate in response to EGF and FGF in the developing mouse telencephalon. *Dev. Biol.* **208:** 166–188.

Tropepe, V., Hitoshi, S., Sirard, C., Mak, T.W., Rossant, J., and van der Kooy, D. 2001. Direct neural fate specification from embryonic stem cells: A primitive mammalian neural stem cell stage acquired through a default mechanism. *Neuron* **30:** 65–78.

Wilson, S.I. and Edlund, T. 2001. Neural induction: Toward a unifying mechanism. *Nat. Neurosci.* **4 (Suppl.):** 1161–1168.

Wood, H.B. and Episkopou, V. 1999. Comparative expression of the mouse *Sox1*, *Sox2* and *Sox3* genes from pre-gastrulation to early somite stages. *Mech. Dev.* **86:** 197–201.

Ying, Q.-L., Stavridis, M., Griffiths, D., Li, M., and Smith, A. 2003. Conversion of embryonic stem cells into neuroectodermal precursors in adherent monoculture. *Nat. Biotechnol.* **21:** 183–186.

THE JOURNAL OF BIOLOGICAL CHEMISTRY
Vol. 279, No. 32, Issue of August 6, pp. 33368–33378, 2004
Printed in U.S.A.

Overexpressed GM1 Suppresses Nerve Growth Factor (NGF) Signals by Modulating the Intracellular Localization of NGF Receptors and Membrane Fluidity in PC12 Cells*

Received for publication, April 6, 2004, and in revised form, May 14, 2004
Published, JBC Papers in Press, May 15, 2004, DOI 10.1074/jbc.M403816200

Masashi Nishio‡, Satoshi Fukumoto‡§, Keiko Furukawa‡, Akiko Ichimura‡, Hiroshi Miyazaki‡, Susumu Kusunoki¶, Takeshi Urano‡, and Koichi Furukawa‡‖

From the ‡Department of Biochemistry II, Nagoya University School of Medicine, 65 Tsurumai, Showa-ku, Nagoya 466-0065, the §Department of Pediatric Dentistry, Nagasaki University School of Dentistry, Sakamoto, Nagasaki 852-8588, and the ¶Department of Neurology, Kinki University School of Medicine, Ohno-Higashi, Sayama, Osaka 589-8511, Japan

Ganglioside GM1 has been considered to have a neurotrophic factor-like activity. To analyze the effects of endogenously generated GM1, the rat pheochromocytoma cell line PC12 was transfected with the GM1/GD1b/GA1 synthase gene and showed increased expression levels of GM1. To our surprise, $GM1^+$-transfectant cells ($GM1^+$ cells) showed no neurite formation after stimulation with nerve growth factor (NGF). Autophosphorylation of NGF receptor TrkA and activation of ERK1/2 after NGF treatment were scarcely detected in $GM1^+$ cells. Binding of ^{125}I-NGF to PC12 cells was almost equivalent between $GM1^+$ cells and controls. However, dimer formation of TrkA upon NGF treatment was markedly suppressed in $GM1^+$ cells in both cross-linking analysis with Bis(sulfosuccinimidyl)suberate 3 and ^{125}I-NGF binding assay. The sucrose density gradient fractionation of the cell lysate revealed that TrkA primarily located in the lipid raft fraction moved to the non-raft fraction in $GM1^+$ cells. $p75^{NTR}$ and Ras also moved from the raft to non-raft fraction in $GM1^+$ cells, whereas flotillin and GM1 persistently resided in the lipid raft. TrkA kinase activity was differentially regulated when GM1 was added to the kinase assay system *in vitro*, suggesting suppressive/enhancing effects of GM1 on NGF signals based on the concentration. Measurement of fluorescence recovery after photobleaching revealed that the membrane fluidity was reduced in $GM1^+$ cells. These results suggested that overexpressed GM1 suppresses the differentiation signals mediated by NGF/TrkA by modulating the properties of the lipid raft and the intracellular localization of NGF receptors and relevant signaling molecules.

Gangliosides, sialic acid-containing glycosphingolipids, are thought to play important roles in the development and function of the nervous system, because they accumulate in brain tissues of vertebrates, and their profiles of carbohydrate moiety alter with development (1, 2). Recently, a number of glycosyltransferase genes have been isolated, and studies of these genes have shown that the various expression patterns of gangliosides are determined basically by the combination of activated glycosyltransferase genes (3). Among complex gangliosides, GM1[1,2] has been most rigorously studied, because it is one of the major gangliosides in vertebrate brain (2) and shows specific binding with the cholera toxin B subunit resulting in important biological events such as cAMP response (4). Since GM1 synthase cDNA was isolated by us (5), the mRNA expression of the gene has been directly examined, and a high expression level in the rat fetal brain has been demonstrated.

Recently, membrane microdomains such as glycolipid-enriched microdomains, detergent-insoluble microdomains, or lipid rafts have been thought of as sites for signal transduction as well as for endocytosis and cholesterol turnover on the cell membrane (6). They are enriched in cholesterol, glycosylphosphatidylinositol-anchored proteins, sphingomyelin, glycosphingolipids, and various signaling molecules such as growth factor receptors, G-proteins, and Src family tyrosine kinases (7). Although ganglioside GM1 has been used as a mere marker of rafts, we demonstrated that GM1 might regulate the signal magnitude of PDGF/PDGFR by altering the intracellular localization of PDGF receptor (R) in Swiss3T3 cells (8). There have also been a number of reports indicating the effects of glycosphingolipids on the growth/differentiation signals (9). These reports suggested that GM1 might affect the structure/function of lipid rafts in neuronal cells, resulting in the regulation of differentiation/proliferation signals.

A rat pheochromocytoma cell line PC12 has been widely used as a differentiation model of neuronal cells, because they show neurite extension after nerve growth factor (NGF) stimulation (10). The effects of NGF are mediated at least in part by TrkA (11), the high affinity NGF receptor containing a tyrosine kinase activity. Mutoh *et al.* (12) demonstrated that GM1 binds to TrkA tightly on the surface of PC12 cells and enhances the effects of NGF (12). Exogenous GM1 enhanced the TrkA phosphorylation and neurite formation when added with a low concentration of NGF. Furthermore, it could rescue PC12 cells

* This work was supported by Grants-in-aid for Scientific Research of Priority Areas 10178104, 10152223, and 10470029, and COE (Center of Excellence) Research from the Ministry of Education, Science, Sports, and Culture of Japan. The costs of publication of this article were defrayed in part by the payment of page charges. This article must therefore be hereby marked "*advertisement*" in accordance with 18 U.S.C. Section 1734 solely to indicate this fact.

‖ To whom correspondence should be addressed. Tel.: 81-52-744-2070; Fax: 81-52-744-2069; E-mail: koichi@med.nagoya-u.ac.jp.

[1] The abbreviations used are: GM1, Galβ1,3GalNAcβ1,4(NeuAcα2,3)-Galβ1,4Glc-ceramide; GM3, NeuAcα2,3Galβ1,4Glc-ceramide; GT1b, NeuAcα2,3Galβ1,3GalNAcβ1,4(NeuAcα2,8NeuAcα2,3)Galβ1,4Glc-ceramide; NGF, nerve growth factor; FBS, fetal bovine serum; PBS, phosphate-buffered saline; FITC, fluorescein isothiocyanate; mAb, monoclonal antibody; MAPK, mitogen-activated protein kinase; ERK(s), extracellular signal-regulated kinase(s); MEK, MAPK/ERK kinase; FRAP, fluorescence recovery after photobleaching; PDGF, platelet-derived growth factor; PDGFR, PDGF receptor; CTB, cholera toxin B subunit; MTT, 3-(4,5-dimethylthiazol-2-yl)-2,5-diphenyltetrazolium bromide; BS3, Bis(sulfosuccinimidyl)suberate; Mes, 2-morpholinoethanosulfonic acid; GEM, glycolipid-enriched microdomain(s).

[2] Ganglioside nomenclature is based on that of Svennerholm (53).

from apoptotic death induced by serum deprivation (13). These results seemed to reflect the neurotrophic nature of GM1. However, it is not clear whether endogenously generated GM1 plays the same roles as exogenous GM1.

In the present study, we established stable transfectant lines of PC12 with the GM1/GD1b/GA1 synthase cDNA, which we had isolated previously (5), and analyzed the response to NGF. To our surprise, marked alterations in the cell response to the induced differentiation and in the activation of signaling molecules were found in GM1$^+$ cells. We also demonstrated dramatic changes in the intracellular localization of NGF receptors and relevant molecules, *i.e.* the majority of TrkA, p75^{NTR}, and Ras moved from the raft to the non-raft fraction in GM1$^+$ cells, whereas the raft markers such as GM1 and flotillin persistently stayed in the raft fraction. These results suggested that GM1 plays critical roles in the regulation of the physicochemical nature of lipid raft and of the bio-signals to determine the cell fates.

EXPERIMENTAL PROCEDURES

Materials—Mouse 2.5S NGF was obtained from Alomone Laboratory (Jerusalem, Israel). Anti-NGF receptor TrkA antibodies (C-14, rabbit IgG; B-3, mouse IgG) and an anti-caveolin-1 antibody were from Santa Cruz Biotechnology (Santa Cruz, CA). Anti-TrkA (rabbit IgG) was from Upstate biotechnology (Lake Placid, NY). Anti-p75 (rabbit IgG) was from Promega (Madison, WI). Anti-flotillin (rabbit IgG) and anti-phosphotyrosine monoclonal antibodies (mAb) (PY20) were from BD Transduction Laboratories (Lexington, KY). Anti-ERK1/2 rabbit IgG, anti-phospho-ERK1/2 rabbit IgG, and anti-rabbit IgG conjugated with horseradish peroxidase were from New England Biolabs (Beverly, MA). An anti-Ras mAb was from Seikagaku Co. (Tokyo, Japan). Cholera toxin B subunit (CTB) conjugated with biotin was from LIST Biological Laboratories (Campbell, CA). CTB-Alexa555 was from Molecular Probe (Eugene, OR). ^{125}I-NGF (~1500 Ci/mmol) was from Amersham Biosciences. Protein A-Sepharose 4 Fast Flow was from Amersham Biosciences. Immobilon-P Transfer Membrane was from Millipore (Bedford, MA). Anti-phospho-TrkA (New England Biolabs) and anti-extracellular domain of TrkA antibodies were purchased from Upstate Biotechnology (Lake Placid, NY).

Recombinant DNA—Human β1,3-galactosyltransferase cDNA clone pM1T-9 (5) was digested with XhoI-XbaI and inserted into the XhoI-XbaI site of pMIKneo to obtain pMIKneo/M1T-9. pMIKneo is a mammalian expression vector with the SRα promoter and was generously presented by Dr. K. Maruyama (Tokyo Medical and Dental University).

Cell Culture and Transfection—PC12 cells were maintained in RPMI 1640 medium supplemented with 10% horse serum and 5% fetal calf serum, at 37 °C in a humidified atmosphere containing 5% CO_2 as described previously (14). PC12 cells used for cDNA transfection were plated in a 60-mm plastic tissue culture plate (Falcon) at a density of 7×10^5 cells/4 ml/plate. The plasmid pMIKneo/M1T-9 (4 μg) was transfected into cells with LipofectAMINE (Invitrogen, Rockville, MD) according to the manufacturer's instructions. Stable transfectant cells were selected in the presence of 250 μg/ml G418 (Invitrogen) and maintained continuously in the presence of G418 (200 μg/ml).

Neurite Outgrowth Assay—PC12 cells and the transfectants were seeded at 1×10^4 cells/well in a type I collagen-coated 48-well culture plate (Falcon) and were either treated with 100 ng/ml 2.5S NGF (Alamone Laboratories) in serum-free medium or left untreated in the serum-containing medium. Neurite-bearing cells were counted for the following 4 days. To analyze the effect of exogenous GM1 on neurite outgrowth, PC12 cells were treated with either serum-free medium or medium containing 100 ng/ml NGF, 5 ng/ml NGF, 50 μM GM1 (Sigma), or 5 ng/ml NGF with 50 μM GM1 (preincubated with 50 μM GM1 for 12 h at 37 °C, then treated with 5 ng/ml NGF). The percentage of cells bearing neurites of various lengths was counted from days 1 to 4.

Flow Cytometry—The cell surface expression of gangliosides was analyzed by flow cytometry (BD Biosciences), using the anti-ganglioside mAbs as described previously (8); mAbM2590 (anti-GM3), mAb10–11 (anti-GM2), mAb92–22 (anti-GD1a), mAbR24 (anti-GD3), mAb220–51 (anti-GD2), mAb370 (anti-GD1b), mAb CDR73–6 (anti-fucosyl-GM1), and mAb549 (anti-GT1b). The cells were incubated with mAbs for 45 min on ice and then stained with FITC-conjugated goat anti-mouse IgM or IgG (Cappel, Durham, NC). To analyze GM1, cells were incubated with the CTB subunit-biotin conjugates (List Biological Laboratories, Inc., Campbell, CA) for 45 min on ice, and then stained with FITC-conjugated avidin (EY Laboratories, San Mateo, CA). Control samples were prepared using the second antibody alone. The intensity of staining was measured and presented in arbitrary units as the log of fluorescent intensity.

MTT Assay—3×10^3 cells were seeded with serum-containing medium in 98-well plates. At 0–5 day of culture, MTT assay was performed as described (8). Growth of cells was quantified by assessing the reduction of MTT to formazan, measured as the absorbance at 590 nm using a plate reader ImmunoMini NJ-2300 (System Instrument, Tokyo, Japan).

Electrophoresis and Immunoblotting—PC12 cells and transfectants were plated in 60-mm tissue culture plates in serum-containing medium, then cells were treated as described below. For the assay of mitogen-activated protein kinase (MAPK) and TrkA phosphorylation, the medium was replaced with serum-free medium and incubated for 1 h. Then cells were incubated with 100 ng/ml 2.5S NGF for 0, 5, 15, 30, 60, and 120 min at 37 °C. After each treatment, the medium was removed, and cells were washed three times with 3 ml of serum-free medium, then solubilized in 200 μl of lysis buffer (10 mM Tris-HCl, pH 7.4, 150 mM NaCl, 10 mM $MgCl_2$, 0.5% Nonidet P-40, 1 mM $NaVO_4$, 1 mM phenylmethylsulfonyl fluoride, 20 units/ml aprotinin). Lysed cells were transferred into microcentrifuge tubes, centrifuged at 3,000 rpm for 10 min, and the supernatant was collected to remove nuclei.

Lysates were separated with SDS-PAGE using 7–12% gels. The separated proteins were transferred onto an Immobilon-P (polyvinylidene difluoride) membrane (Millipore). Blots were blocked with 10% skim milk in phosphate-buffered saline (PBS) for 1 h. The membrane was first probed for 1 h with primary antibodies at the dilution suggested by the suppliers. After washing three times with PBST (0.05% Tween 20 in PBS), the blots were then incubated for 1 h with goat anti-rabbit IgGs or goat anti-mouse IgGs conjugated with horseradish peroxidase (1:4000). After the membranes were washed three times with PBST, bound conjugates were visualized with an ECL detection system (PerkinElmer Life Science). For detection of GM1, the membranes were probed with CTB-biotin (1:500) and detected with an ABC kit (Vector Laboratories). To analyze the effects of the reduced GT1b expression, the transfectant cells were cultured with exogenous GT1b (50 μM) and used for immunoblotting as described above after confirmation of GT1b incorporation on the cell surface with flow cytometry.

Immunoprecipitation—Cells were lysed with lysis buffer (10 mM Tris-HCl, pH 7.4, 10 mM EDTA, 1% Nonidet P-40, 0.4% deoxycholate, 60 mM β-octylglucoside, 1 mM phenylmethylsulfonyl fluoride, 1 mM Na_3VO_4, 0.1 mg/ml aprotinin). After sonication (3 × 20 s), insoluble material was removed by centrifugation at 4 °C (10,000 × *g* for 2 min). The lysate was incubated with antibodies at 4 °C overnight. The immune-complex was precipitated after incubation with protein A-Sepharose (Amersham Biosciences) for 2 h. The beads were washed three times with the lysis buffer, and the precipitates were solubilized in a Laemmli sample buffer by heating for 3 min at 98 °C.

TrkA Receptor Cross-linking—Cells were plated at a density of 6×10^6/10-cm dish, and serum-starved for 1 h before NGF treatment. Then, cells were washed with plain medium without serum and treated with NGF (50 ng/ml) for 5 min at 37 °C. The medium was removed, and cells were washed twice with ice-cold PBS, and then cross-linked using 1 mM BS3 in a cross-linking buffer (25 mM HEPES, pH 8.5, 120 mM NaCl, 6 mM KCl, 1 mM $MgCl_2$, 10 mM EGTA) at 4 °C for 1 h. The cross-linking reaction was terminated by adding 1 M Tris-HCl (pH 7.4) to a final concentration of 0.1 M. Then, cells were washed twice in Tris-buffered saline and lysed in the lysis buffer as described above. TrkA was immunoprecipitated, and immunoprecipitates were separated on a 7% gel with an acrylamide/bisacrylamide ratio of 200:1. Samples were transferred onto membranes and immunoblotted with an anti-Trk antibody (B-3).

Isolation of Raft Fraction—Microdomain rafts were prepared using a non-detergent extraction method essentially as described by Song *et al.* (15). Cells were plated at a density of 2×10^7/15-cm dish and cultured up to 90% confluency, and five dishes of cells were used for each preparation. After being washed twice with ice-cold PBS, the cells were scraped in 1 ml of 0.5 M sodium carbonate buffer, pH 11.0. The cells were homogenized sequentially using a loose fitting Dounce homogenizer (10 strokes), a Polytron tissue grinder (three 10-s bursts), and a sonicator (three 20-s bursts). All procedures were carried out at 4 °C. The homogenate (1 ml) was then adjusted to 45% (w/v) sucrose by adding 1 ml of 90% (w/v) sucrose prepared in 2× MNE buffer (25 mM Mes, pH 6.5, 150 mM NaCl, 5 mM EDTA). The final pH of the mixture was 10.2. A discontinuous sucrose gradient was formed by overlaying 2 ml of 35% (w/v) sucrose onto the mixture, and then 1 ml of 5% (w/v) sucrose was overlaid. Both of these layers were prepared with MNE

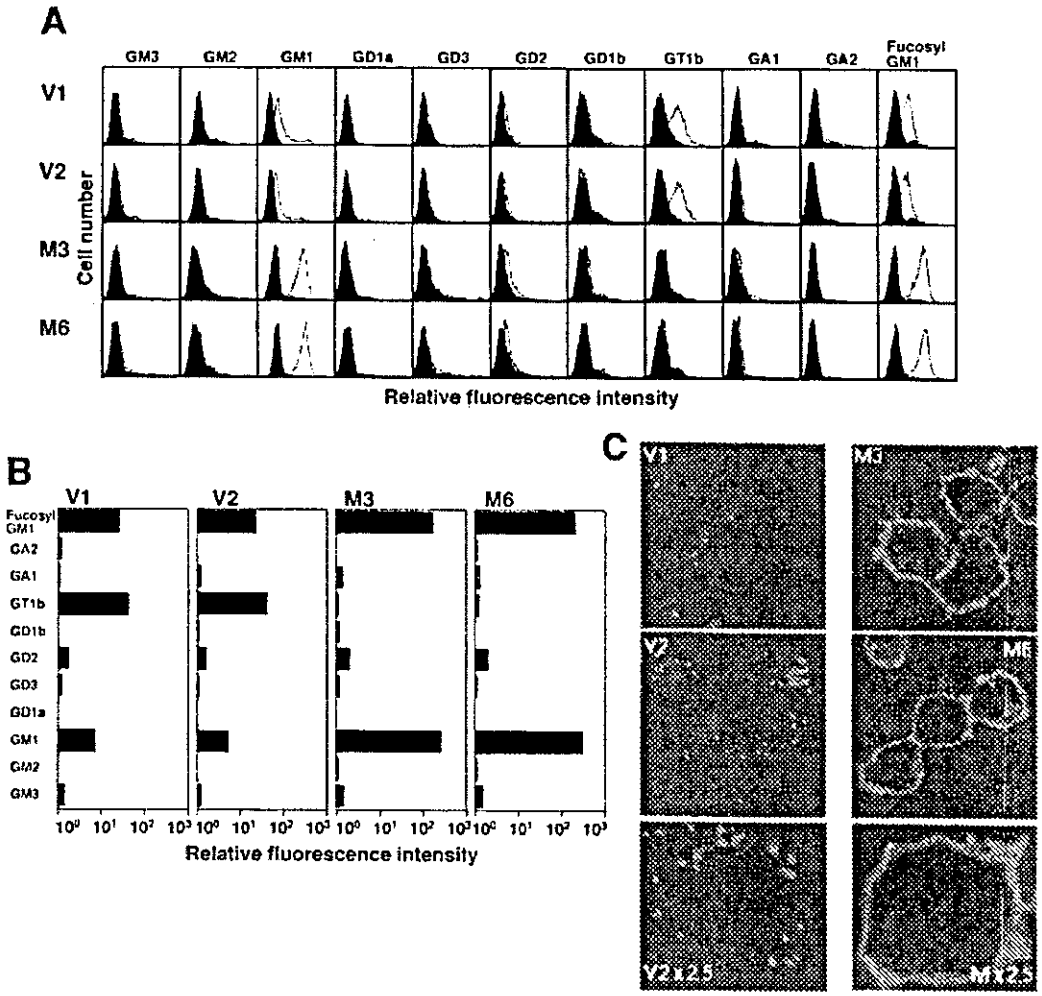

FIG. 1. **Expression levels of gangliosides in the transfectant cells.** The cell surface expression levels of gangliosides in each cell line were analyzed by flow cytometry. *A*, actual flow cytometric patterns of gangliosides examined are presented. Cells were stained with the anti-ganglioside mAbs. Controls were prepared with second antibody alone and presented by *thin lines* with *dark shading*. *B*, expression levels of gangliosides are shown on the basis of mean fluorescence intensities. The mean fluorescence values with individual antibodies were subtracted with those of corresponding controls. The expression levels of gangliosides were indicated in the *abscissa* with logarithm. *V1* and *V2* are vector control cells transfected with a vector alone, and *M3* and *M6* are $GM1^+$ cells. *C*, to compare the distribution pattern of GM1 in the cells, we used CTB-Alexa555 for staining cell surface GM1. Whereas GM1 showed the patched distribution in vector control cells, it was distributed throughout the plasma membrane with much stronger intensity in $GM1^+$ cells. The original magnification is ×400, and *two panels* at the *bottom* are 2.5-fold more magnified.

containing 0.25 M sodium carbonate. The samples were centrifuged at 20,000 × *g* in an SW50.1 rotor for 16 h at 4 °C. From the top of the gradient, 0.5 ml of each fraction was collected to yield 10 fractions. The components in each fraction were concentrated by centrifugation at 100,000 × *g* for 2 h at 4 °C in MNE buffer, and precipitates were resolved in the lysis buffer and used for immunoprecipitation or Western immunoblotting.

NGF-TrkA Cross-linking—Cells were resuspended in a binding buffer (Hanks' containing 1 mg/ml each of glucose and bovine serum albumin) at 5 × 10^6 cells/ml and incubated at 4 °C for 1 h with 1 nM ^{125}I-NGF (2750 dpm). To correct the nonspecific binding, unlabeled NGF (1 μM) was added during the binding. To cross-link NGF with TrkA, BS3 was added to a final concentration of 1 mM to the reaction mixture, and the mixture was incubated at 4 °C for 1 h. After the cross-linking reaction was terminated, cells were washed and lysed in the lysis buffer. The lysates were used for immunoprecipitation with an anti-Trk antibody, and the immunoprecipitates were separated using a 7% gel as described above. ^{125}I-NGF-bound proteins were detected with autoradiography using an imaging plate and BAS2000 Bioimage Analyzer™ (Fujifilm, Tokyo).

NGF Binding Assay—Cells were resuspended in a binding buffer at 1 × 10^5 cells/0.2 ml and incubated at 37 °C for 45 min with various concentrations (5 pM to 10 nM) of ^{125}I-NGF. The reaction mixture was overlaid onto 5% bovine serum albumin in 0.32 M sucrose and was centrifuged at 10,000 × *g* for 1 min at 4 °C. The supernatants were collected, and the tips of tubes containing the cell pellets were cut off. A 1,000-fold excess of unlabeled NGF was used to assess the nonspecific binding. The radioactivity was counted in a γ-counter, and the results were analyzed on the basis of Scatchard plot.

In Vitro Kinase Assay—The PC12 lysate was used for immunoprecipitation with an anti-TrkA antibody as described above. Immunoprecipitates were washed twice with the lysis buffer and twice with the Tris-buffered saline containing a phosphatase inhibitor (100 μM Na_3VO_4). Immunoprecipitates were resuspended in a tyrosine kinase assay buffer (50 mM HEPES, pH 7.4, 20 mM $MnCl_2$, 5 mM $MgCl_2$, 1 mM dithiothreitol, 100 μM Na_3VO_4, 5 μCi/sample [γ-^{32}P]ATP) and then incubated for 10 min at 30 °C in the presence of various concentrations of GM1. The kinase reaction was terminated by adding Laemmli sample buffer followed by boiling. Relative kinase activity was measured by scanning the bands in the autoradiogram as described above. The effects of GM3 or GT1b were also examined for comparison.

Immunofluorescence Study—Cells were cultured on a poly-L-lysine-coated coverslip, and cells were fixed with 4% paraformaldehyde in PBS. Then, cells were treated with CTB-Alexa555 (10 μg/ml) in PBS for 1 h at 4 °C. The fixed cells were analyzed with a confocal laser microscope Fluoview FV500™ (Olympus, Tokyo).

Rho Kinase Assay—To determine the alteration in the activation levels of Rho, activated Rho was isolated and analyzed with the method

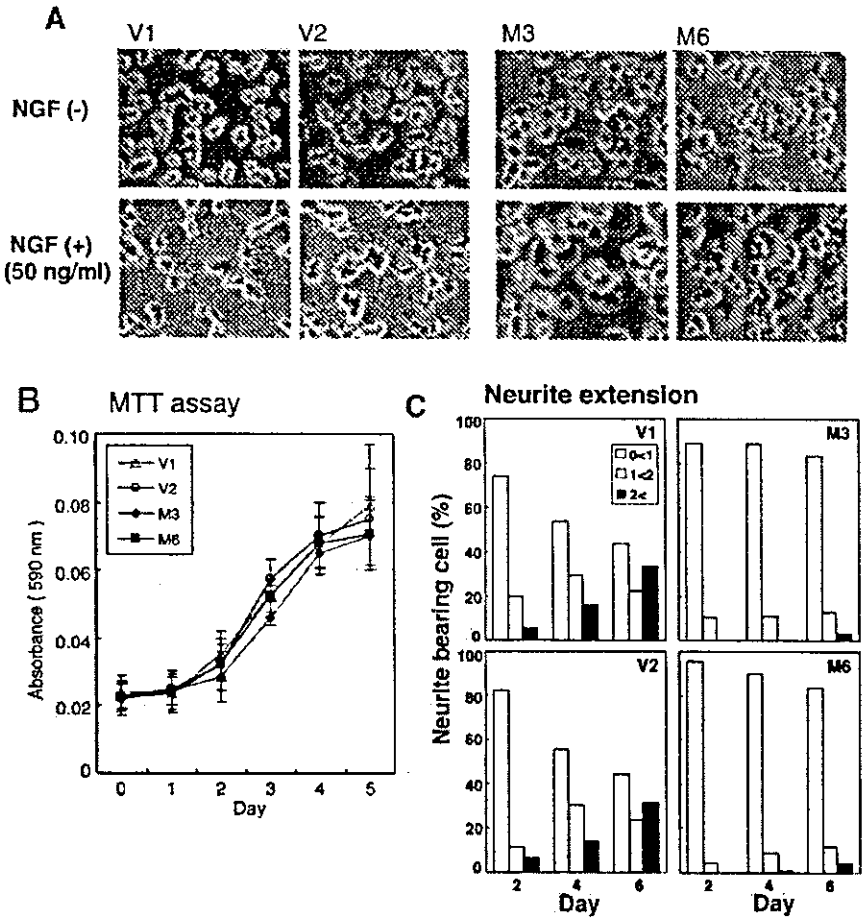

FIG. 2. **Differentiation and proliferation of GM1 synthase gene transfectants.** *A*, response to NGF of vector control cells and GM1 synthase gene transfectants. Phase contrast micrographs of cells cultured in the absence (*upper*) or presence (*under*) of 50 ng/ml NGF for 5 days are shown. *B*, cell proliferation as analyzed with MTT assay. Cells were seeded in 96-well plates for MTT assay. The data shown are the mean ± S.D. from five samples. *C*, time course of the neurite extension after NGF treatment (50 ng/ml). The percentage of cells bearing neurites of lengths more than 2-fold of the cell diameter (*closed bars*), less than 2-fold lengths (*hatched bars*), and of those with no neurites (*open bars*) are presented (n = 50).

of Ren *et al.* (16) using a Rho Activation Assay kit (Cytoskeleton, Denver, CO) according to the manufacturer's instruction. Cells were plated at a density of 6×10^6/10 cm dish. After being washed, cells were lysed with lysis buffer, and the cell lysates were centrifuged at 10,000 × *g* for 5 min at 4 °C, and the supernatants were incubated with Rhotekin-RBD beads under rotation for 1 h at 4 °C. The beads were washed three times with the lysis buffer, and the precipitates were solubilized in a Laemmli sample buffer, heated for 3 min at 98 °C, and then separated in SDS-PAGE. Bound Rho proteins were detected by Western immunoblotting using an anti-Rho polyclonal antibody in the kit.

Measurement of the Membrane Fluidity by Fluorescence Recovery after Photobleaching—Cells were cultured on a glass bottom dish coated with poly-D-lysine, and the medium was replaced with a standard external solution (10 mM Hepes, 150 mM NaCl, 5 mM KCl, 2 mM $CaCl_2$, 1 mM $MgCl_2$, 10 mM glucose) prewarmed at 37 °C. A fluorescent probe, DiI (DiIC_{18}; D-282, Molecular probes, Eugene OR) was added to the standard external solution at 2.5 μg/ml and incubated for 10 min, to be incorporated into the cell membranes. FRAP analyses were performed with a confocal laser scanning microscope (Olympus) equipped with a stage heater at 37 °C. A small area of the labeled membrane was photobleached by full laser power (100%), resulting in the immediate reduction of the intensity of fluorescence. A selected area (3-μm square) on the labeled cell membrane was photobleached for 8–15 s by a 488-nm laser beam. Then, the fluorescence recovery in the photobleached area was immediately recorded using a time-lapse option of the system until the fluorescence was recovered at a plateau level. Relative recovery in fluorescence intensity was calculated for 60 s after photobleaching and analyzed by Microsoft Excel. FRAP was calculated by a ratio of post-bleach intensity/pre-bleach intensity, and the membrane fluidity was evaluated by comparing the percentage of FRAP to a plateau as follows. Fluorescence intensities at a pre-photobleach state and the post-photobleach intensities at a plateau were expressed as average values of 10 scans. In each experiment, the value obtained at pre-photobleach was taken as 100% and that at just after photobleach was taken as 0% to compensate for the differences among experiments. The half-maximal recovery of fluorescence ($t_{1/2}$) was also calculated on the basis of the duration (t) of fluorescence recovery reaching a plateau.

RESULTS

Expression of Gangliosides in GM1 Synthase Gene Transfectant Cells (GM1$^+$ Cells)—After the transfection of PC12 cells with a GM1 synthase gene expression vector (pMIKneo/M1T-9), or pMIKneo, two transfectant lines (M1 and M3) and two vector controls (V1 and V2) were established, respectively. Expression profiles of gangliosides were examined by flow cytometry (Fig. 1*A*). The mean fluorescence values of individual gangliosides obtained by subtracting those of corresponding controls are shown in Fig. 1*B*. Among the gangliosides examined, expression levels of GM1 and fucosyl-GM1 markedly increased in the transfectants (M3 and M6). Expression levels of other gangliosides showed no apparent change compared with those in the vector control lines (V1 and V2) except that GT1b expression level reduced after the transfection. To compare the distribution pattern of GM1 on the cell membrane, we stained the cultured cells with CTB-Alexa555. Whereas GM1 in vector control cells showed a weak and patched distribution, those in the GM1$^+$ cells showed very strong staining and a uniform and thick distribution throughout the plasma membrane (Fig. 1*C*).

No Neurite Extension with NGF in PC12 Cells Transfected with GM1 Synthase cDNA—To examine the effects of GM1 expressed endogenously on NGF-induced differentiation, the GM1$^+$ cells and vector controls were cultured with or without 50 ng/ml NGF for 5 days. Fig. 2 shows the morphological change in controls and GM1$^+$ cells after 5 days of NGF treatment. As reported previously, cell proliferation was reduced

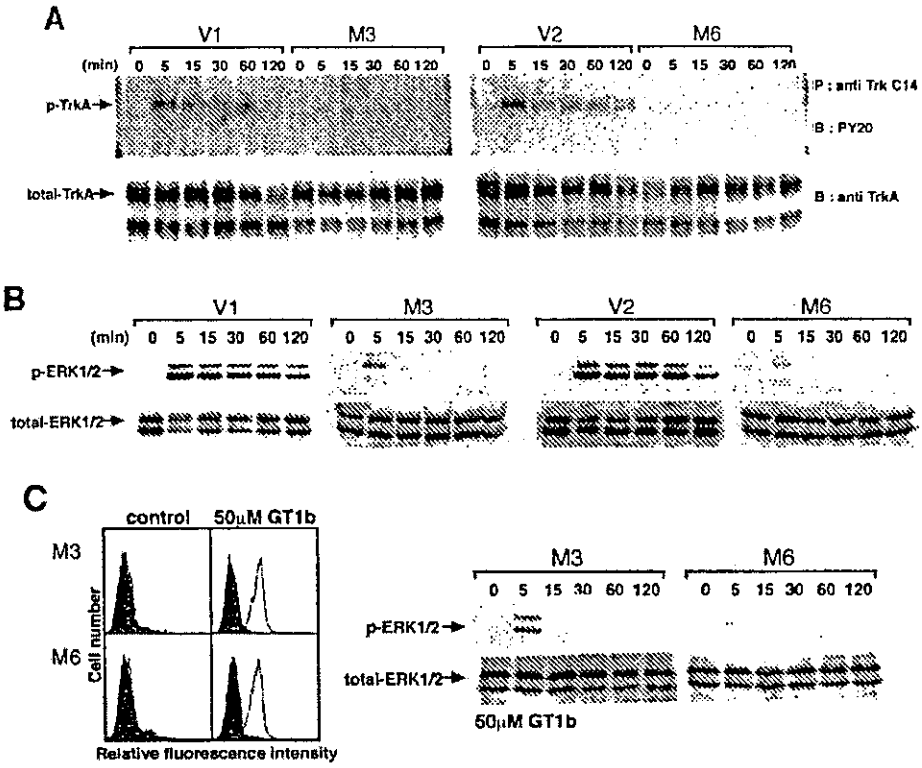

FIG. 3. **Reduced phosphorylation of TrkA and ERK1/2 after NGF treatment in the transfectant cells.** *A*, time courses of the phosphorylation levels of TrkA in the vector controls (*V1* and *V2*) and the GM1$^+$ cells (*M3* and *M6*) were analyzed. Cells were treated with NGF (50 ng/ml) for the times indicated. TrkA was immunoprecipitated with an anti-Trk antibody (*C-14*), and immunoblotting was carried out using PY-20 (*upper*) or anti-TrkA antibody (*bottom*). *B*, activation of ERK1/2. Cells were treated as described in *A* and were then lysed with Nonidet P-40 lysis buffer, and total lysates were separated by 12% SDS-PAGE. Western blotting was carried out using an anti-phosphorylated ERK1/2 antibody (*upper*) or an anti-ERK1/2 (*lower*). A similar experiment was repeated, and essentially similar results were obtained. *C*, GM1 synthase gene transfectants were treated with GT1b (50 μM) for 4 h, and the cell surface GT1b was detected with flow cytometry (*left*). Then, phosphorylation of ERK1/2 after NGF treatment was examined as described above (*right*). Note that there are no differences between M3 and M6 in *B* and those in *C*.

and neurite formation was observed in vector control cells (Fig. 2*A*). In contrast, the GM1$^+$ cells showed no neurite extension, although cell proliferation was not affected (Fig. 2, *A* and *B*). Quantitative analysis of the neurite formation revealed that only 10–20% of GM1$^+$ cells showed neurites longer than twice the cell diameter even on day 4 of culture (Fig. 2*C*). On the other hand, 80% of control cells showed neurites longer than twice the diameter. Although the vector controls showed little neurite outgrowth when treated with low density of NGF (5 ng/ml), the pretreatment with GM1 (50 μM) enhanced the outgrowth as previously reported (12, 13) (data not shown). In contrast, GM1$^+$ cells showed no neurite outgrowth even when stimulated with a high concentration of NGF (100 ng/ml) (data not shown).

Reduced Phosphorylation of TrkA and ERKs with NGF Treatment—It has been known that exogenously added GM1 enhanced NGF-induced neurite extension. To determine the effects of the overexpressed GM1 on NGF-derived signals in the GM1$^+$ cells, the time course of tyrosine phosphorylation of Trk after NGF treatment was investigated. Tyrosine phosphorylation of TrkA was detected at 5 min after NGF treatment and gradually reduced in the control cells (Fig. 3*A*). On the other hand, tyrosine phosphorylation of TrkA was scarcely detected in the GM1$^+$ cells. As for the downstream ERK1/2 phosphorylation, only weak phosphorylation was found at 5 min after the NGF stimulation in the GM1$^+$ cells correspondingly with the reduced phosphorylation of TrkA (Fig. 3*B*). In the control cells, the phosphorylation of ERK1/2 was clearly detected at 5 min after NGF treatment with subsequent slow reduction. Immunoblots with anti-ERK1/2 antibody demonstrated that applied lysates contained equivalent amounts of ERK proteins (Fig. 3*B*, *bottom panels*). To examine the effects of the reduced GT1b expression level in the GM1$^+$ cells, the transfectant cells were cultured in the presence of exogenous GT1b and were analyzed for the phosphorylation of ERK1/2. GT1b was well incorporated on the membrane (Fig. 3*C*). The phosphorylation patterns of ERK1/2 after NGF stimulation showed no change after GT1b incorporation, suggesting that the reduced NGF signals in the GM1$^+$ cells were not due to the loss of GT1b expression.

NGF Binding Was Equivalent between the Controls and GM1$^+$ Cells—Using gradually diluted ^{125}I-labeled NGF, NGF binding to the controls and to the GM1$^+$ cells was investigated as described under "Experimental Procedures." Nonspecific binding of ^{125}I-labeled NGF was determined by adding excess amounts (×1000) of cold NGF, and the values were used to subtract from the individual counts. The ^{125}I-labeled NGF specifically bound to PC12 cells in a dose-dependent manner. The Scatchard plots indicated that PC12 cells express two kinds of NGF receptors, *i.e.* a high affinity receptor and a low affinity receptor, as previously reported. B_{max} values calculated from the high affinity binding curves were 2.52×10^2 pmol/10^5 cells and 2.62×10^2 pmol/10^5 cells for V1 and V2, respectively. Those for M3 and M6 were 2.08×10^2 pmol/10^5 cells and 2.44×10^2 pmol/10^5 cells, respectively (Fig. 4). In addition, the dissociation constants (K_d values) of NGF were 0.55 and 0.53 nM for V1 and V2, respectively, and K_d values for M3 and M6 were 0.46 and 0.55 nM, respectively (Fig. 4). There were no significant differences in the binding levels and kinetics between the

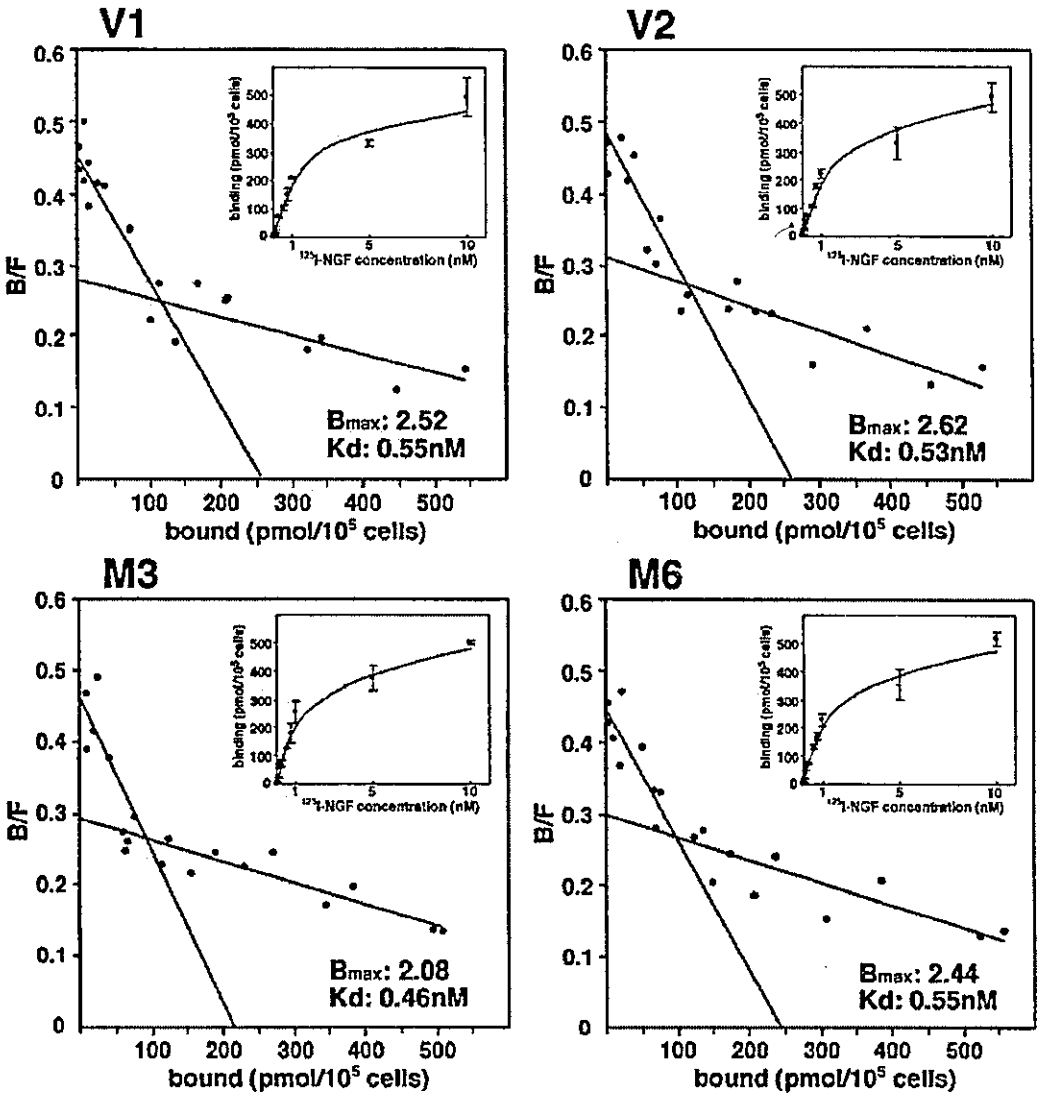

FIG. 4. **NGF binding was equivalent between the controls and GM1$^+$ cells.** Using gradually diluted ^{125}I-labeled NGF, NGF binding to the vector controls and GM1$^+$ cells were investigated. Two vector control cells and two GM1$^+$ cells were analyzed. Nonspecific binding was obtained by adding 1000-fold excess amounts of unlabeled NGF, and the values were used for the subtraction. Scatchard plot analysis was performed, and the results of individual samples are presented. *Insets* are the binding curves, Note that there is no significant difference in the binding kinetics between the controls and GM1$^+$ cells. B_{max} values calculated from the high affinity binding curves are expressed with the unit ($\times 10^2$ pmol/10^5 cells) in the individual figures.

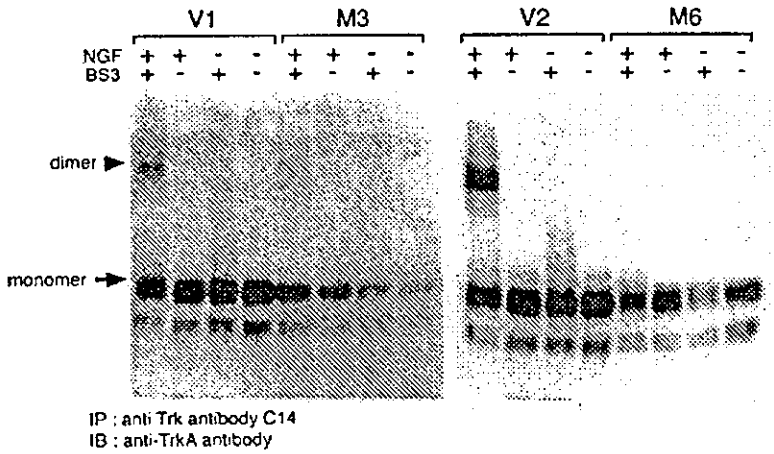

FIG. 5. **Reduced dimerization of TrkA with NGF treatment in GM1 synthase gene transfectant cells.** The cell surface proteins were cross-linked with BS3 under NGF treatment as described under "Experimental Procedures." After cross-linking, TrkA was immunoprecipitated and detected by immunoblotting using an anti-TrkA antibody. The results were reproducible in three independent experiments. The *arrow* represents the TrkA monomer; *arrowhead*, TrkA dimer.

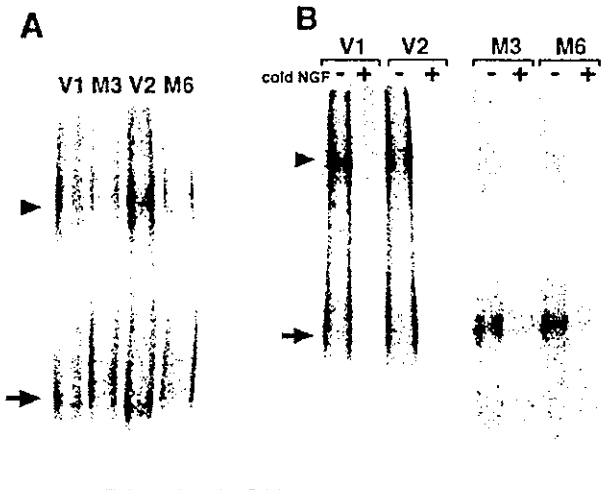

FIG. 6. **Reduced dimerization and binding of dimers with NGF in the transfectant cells as shown with ligand-receptor cross-linking.** Cells were incubated with ^{125}I-NGF (1 nM) at 4 °C for 1 h and then with a cross-linker BS3 for 1 h. TrkA was immunoprecipitated and analyzed. *A*, bands represent TrkA bound with ^{125}I-NGF. TrkA monomer (*arrow*) and dimer (*arrowhead*) were found in vector control cells (*lanes 1* and *3*), whereas mainly monomer form of TrkA was detected in GM1$^+$ cells. *B*, an evidence for the binding specificity. When binding was carried out in the presence of a 1000-fold excess of unlabeled NGF (indicated with "+"), the bands completely disappeared, suggesting that NGF specifically bound to TrkA.

control cells and the GM1$^+$ cells, suggesting that overexpressed GM1 did not disturb the NGF binding itself.

Reduced Dimerization of TrkA with NGF Treatment in the GM1$^+$ Cells—The GM1$^+$ cells showed neither neurite extension nor signal activation after NGF treatment. Then, TrkA dimerization after NGF treatment was investigated. The cell surface proteins were cross-linked with BS3 under the NGF treatment as described under "Experimental Procedures." After cross-linking, TrkA was immunoprecipitated from the cell lysates, and separated in a 7% gel followed by immunoblotting using anti-TrkA antibody (B-3). The immunoblotting showed high molecular mass bands (about 300 kDa) corresponding to TrkA dimer at 5 min after NGF treatment in control cells. On the other hand, the dimer bands of TrkA were scarcely found in the GM1$^+$ cells (Fig. 5).

Reduced Complex Formation between TrkA Dimer and NGF in the Transfectants—Based on the reduction in the phosphorylation and dimerization of TrkA in the GM1$^+$ cells, we questioned whether NGF binding to TrkA is attenuated by overexpression of GM1. The simple binding assay showed no differences as shown in Fig. 4. Then, the dimer formation was markedly reduced in GM1$^+$ cells (Fig. 5). Therefore, we examined NGF binding to TrkA monomer and dimer with cross-linking experiment. Cells were incubated with ^{125}I-NGF (1 nM) at 4 °C for 1 h, and then with a cross-linker BS3 for 1 h. TrkA was immunoprecipitated and analyzed by SDS-PAGE and autoradiography. Radioactive bands, corresponding to the ^{125}I-NGF-bound TrkA monomer (~150 kDa) and ^{125}I-NGF-bound dimer (~300 kDa), were found in vector control cells (Fig. 6*A*).

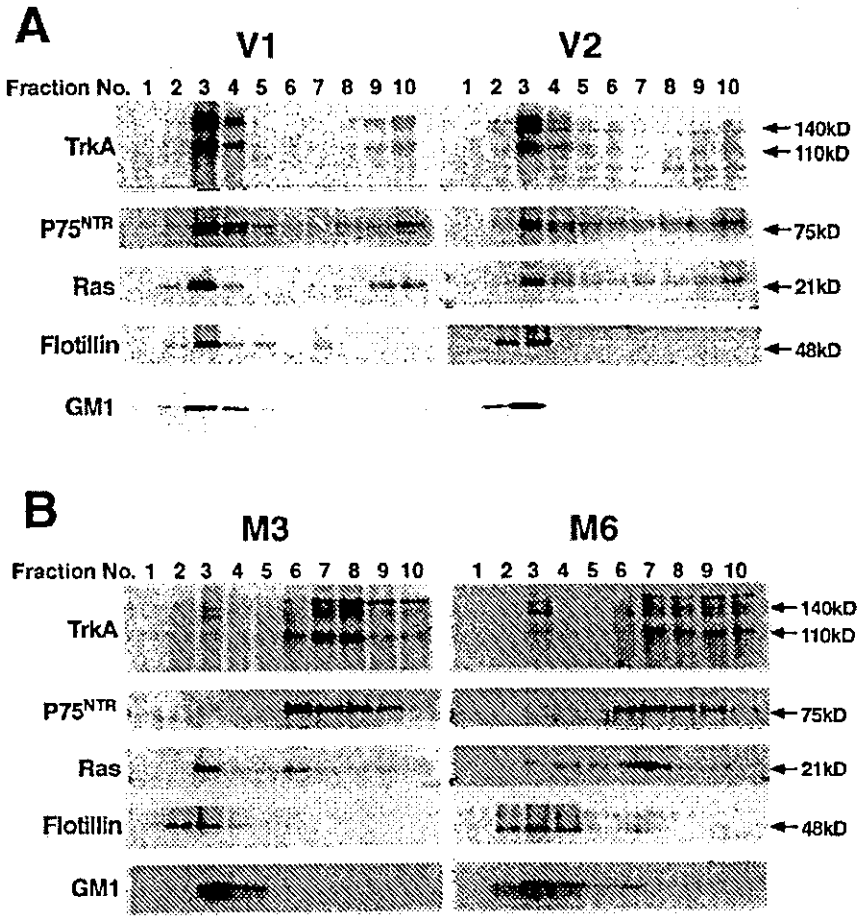

FIG. 7. **Alteration in the flotation in a sucrose gradient of NGF receptors in the GM1$^+$ cells.** Cells were lysed under detergent-free conditions, and the extracts were fractionated. Fractions were subjected to immunoblotting analysis using the antibodies against the proteins indicated. GM1 was detected with CTB. *A*, the results of vector control cells. *B*, the results of GM1$^+$ cells. Note an increased ratio of TrkA and P75^{NTR} in non-raft fractions (6–10) in the GM1$^+$ cells.

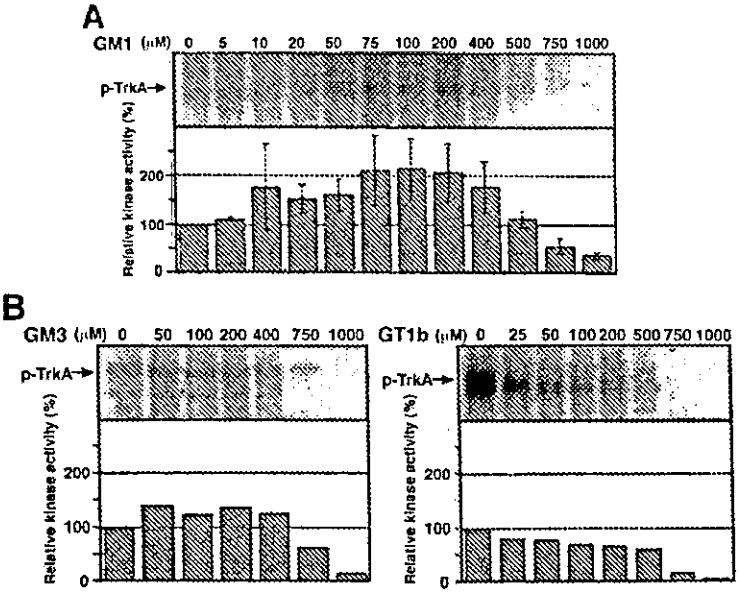

FIG. 8. **GM1 differently affects TrkA tyrosine kinase activity *in vitro*.** Immunoprecipitation with anti-Trk antibody was performed. Immunoprecipitated TrkA was mixed with various concentrations of GM1 (*A*), GM3 or GT1b (*B*), and its kinase activity was measured by adding [γ-^{32}P]ATP and incubating for 10 min at 30 °C, followed by SDS-PAGE and autoradiography. Relative intensity of each band was measured by National Institutes of Health Image and presented as the percentage of the sample with no GM1 (100%). The data shown are the mean ± S.D. from three experiments.

In contrast, dimer bands were hardly detected in GM1$^+$ cells, whereas the band intensities of the monomer were equivalent with those in the controls. These findings indicated that the monomer form of TrkA in the GM1$^+$ cells binds with NGF at the similar level with that in the control cells, although the transfectant cells could not form TrkA dimer or could not bind with NGF, if present. Taken together with the results in Fig. 5, the former case appeared more likely. When binding was carried out in the presence of a 1000-fold excess of unlabeled NGF (Fig. 6*B*), all bands completely disappeared, suggesting that NGF specifically bound to TrkA.

Alteration in the Flotation in a Sucrose Gradient of NGF Receptors in GM1 Synthase Gene Transfectant Cells—Because GM1 has been considered to be localized in lipid rafts, overexpression of GM1 may affect the nature of rafts. Then, we examined the effects of GM1 overexpression on the intracellular localization of NGF receptors (TrkA and p75^{NTR}) by isolating lipid rafts with a detergent-free method. Ten fractions from the discontinuous sucrose gradient were prepared and analyzed for distribution of p75^{NTR}, TrkA, and raft markers, such as flotillin. The distribution of Ras as well as GM1 was also analyzed. Immunoblot analysis showed that most of flotillin, Ras, and GM1 were found in fractions 3 and 4 containing the raft fraction (Fig. 7*A*). The majority of TrkA and p75^{NTR} were also detected in this raft fraction. These results indicated that PC12 cells contained the lipid raft in buoyant density, GM1 content, and protein constituents. To our surprise, the distribution pattern of TrkA and P75^{NTR} dramatically changed in the GM1$^+$ cells (Fig. 7*B*). The main portions of TrkA and p75^{NTR} were detected in the non-raft fraction comprising fractions 6–10, suggesting that the distribution of NGF receptors are strongly affected with the expression levels of GM1, probably based on the modification of the properties of GEM/rafts. The Ras protein also moved in part from the raft to the non-raft fraction, whereas GM1 and flotillin consistently existed in the raft fraction.

GM1 Differentially Regulates TrkA Tyrosine Kinase—To analyze direct effects of GM1 on the TrkA kinase activity, immunoprecipitated TrkA was used for the *in vitro* kinase assay in the presence of various concentrations of GM1. As shown in Fig. 8*A*, low concentrations of GM1 rather enhanced the kinase activity, whereas relatively high concentrations of GM1 (>500 μM) suppressed the kinase in a dose-dependent manner. To examine the specificity of GM1 in the enhancing effect on the TrkA kinase activity, GM3 or GT1b was also added to the kinase assay system at various concentrations (Fig. 8*B*). Consequently, as shown in Fig. 8*B*, clearly neither GM3 nor GT1b enhanced TrkA activity at any concentration as GM1 did.

Rho Is Not Modulated in the GM1 Synthase Gene Transfectants—Because RhoA has been shown to be involved in the regulation of neuronal differentiation and neurite outgrowth (17), overexpression of GM1 might suppress the neurite extension by modulating the Rho activity. Then, we examined the activation level of Rho in the GM1 synthase gene-transfectant cells. Activated Rho was not detected in either the vector controls or the GM1$^+$ cells, although LPA could induce an activated Rho band (data not shown). Therefore, it was not likely that GM1 affected the Rho kinase activity in the transfectant cells.

High Expression of GM1 Resulted in the Reduction of Membrane Fluidity—Because the GM1$^+$ cells showed reduced dimerization of the TrkA receptor (Figs. 5 and 6), and an altered intracellular localization of TrkA receptors (Fig. 7), we thought that overexpression of GM1 might affect the membrane fluidity. Then, we examined the effects of overexpression of GM1 on the plasma membrane fluidity in live cells using a FRAP system as described under "Experimental Procedures." To examine the membrane fluidity in living cells with FRAP experiments, we stained cell surface GM1 by using CTB-Alexa555. As shown in Fig. 1*C*, GM1$^+$ cells were stained uniformly and strongly, and vector control cells showed patched distribution with low intensity. Furthermore, CTB-Alexa555 rapidly underwent endocytosis within 5–10 min, causing troubles to compare FRAP between these two cell types. In contrast, cell surface membranes were uniformly and moderately stained with DiI in both the vector controls and GM1$^+$ cells. Therefore, we used DiI instead of CTB-Alexa555 for cell surface labeling in FRAP experiments. Cells were loaded with 2.5 μg/ml DiI for 10 min, then photobleach was applied to plasma membrane and the fluorescence recovery in these bleached regions was monitored. Fluorescence of DiI was markedly lost after photobleaching, and recovery was observed for ~60 s after photobleaching. Although the fluorescence recovery of membrane in vector control cells was 41.37%, the recovery in the GM1$^+$ cells was 24.8% (Fig. 9*B*). The $t_{1/2}$ values of fluorescence recovery were 7.27 ± 1.9 s and 9.36 ± 2.8 s for vector control and GM1 synthase gene transfectants, respectively (Fig. 9*C*).

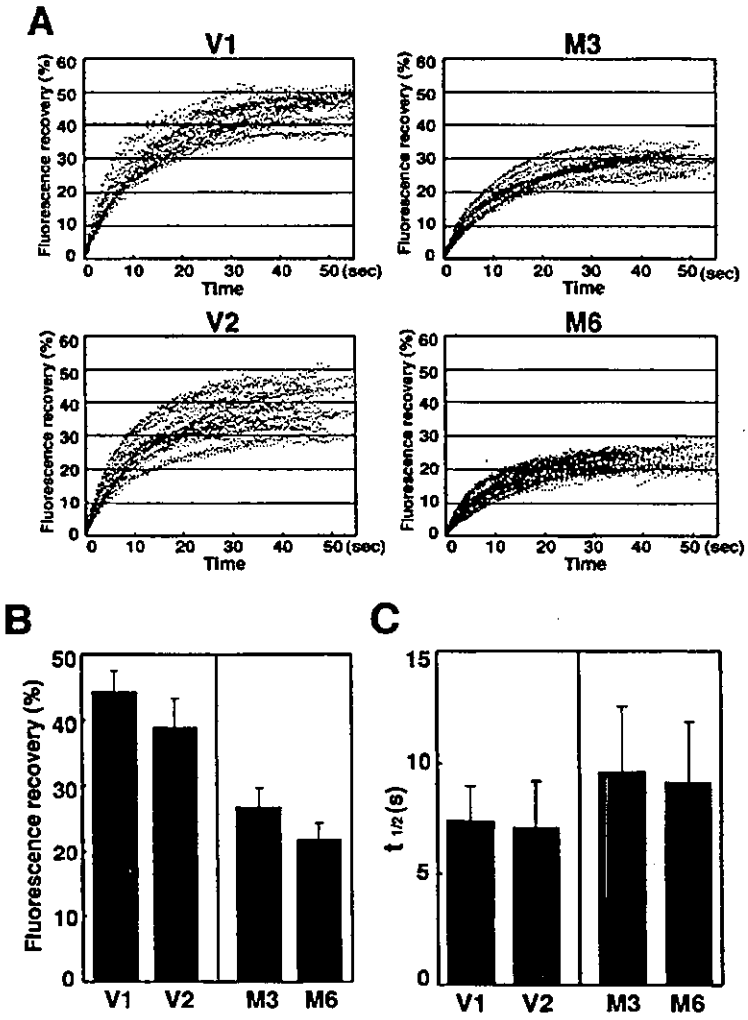

FIG. 9. **High expression of GM1 reduced plasma membrane fluidity of PC12 cells.** The membrane fluidity was monitored using FRAP analysis of the lateral diffusion of incorporated DiI in the plasma membrane of the living cells. *A*, bleaching recovery pattern is presented as the percentage of FRAP. Data are the sum of 30 experiments. *B*, percentages of the fluorescence recovery at the plateau levels in the individual groups. The data shown are the mean ± S.D. from 30 experiments. Comparison between either one of the controls and either one of the transfectants showed significant differences ($p < 0.05$). *C*, the $t_{1/2}$ of the fluorescence recovery (s), *i.e.* the times (seconds) reaching the medial (50%) levels of the plateau in the individual groups were obtained. The data are expressed as the mean ± S.D. of 30 experiments. There was a significant difference between vector controls and GM1$^+$ cells ($p < 0.05$).

These data suggested that overexpression of GM1 reduced the membrane fluidity and might result in the interference with the dimerization and phosphorylation of TrkA.

DISCUSSION

The characteristic expression patterns of gangliosides in the nervous tissues during development have suggested that they play important roles in the neurogenesis of vertebrates (18). Glycosyltransferase genes responsible for the synthesis of gangliosides also showed corresponding expression patterns during brain development (19). Because exogenously added gangliosides induced differentiation of neuronal cells *in vitro* (20), various gangliosides are thought to have neurotrophic effects, and have been administrated to experimental animals after generating artificial neurological damages or disorders by mechanical or chemical manipulation (21), by the injection of toxic reagents (22) or by ischemic treatment (23). Although various gangliosides have often had positive effects presumably due to their neurotrophic activity, it has been difficult to elucidate the molecular mechanisms for the effects of gangliosides endogenously generated in the cells or tissues.

A number of studies have been performed to investigate the effects of gangliosides on the function of nerve growth factor receptors (12, 13, 24–27). Physical and functional association of GM1 with NGF receptor TrkA was reported (24–26). Activation of TrkA with GM1 (24, 26), or enhancement of the TrkA dimerization due to NGF with GM1 (25) was also reported. Ferrari *et al.* (13) reported that GM1 alone could at least partly replace the activity of NGF. In particular, Mutoh *et al.* (12) reported that exogenously added GM1 tightly binds to TrkA and enhances the phosphorylation of TrkA when stimulated with NGF. Rabin *et al.* (27) showed that GM1 activated Trk receptors via the induction of neutrophin release. However, it is not clear whether exogenously added GM1 actually acts in the same way as endogenously generated GM1, because the density and molecular topology of the added GM1 on the cell membrane are hard to be determined. Its molecular form and effect in the liquid on the cultured cells are also difficult to be precisely determined.

Using a cloned GM1/GD1b/GA1 synthase gene (5), we have tried to modify the ganglioside composition of PC12 cells and succeeded in obtaining clones expressing higher levels of GM1. Although the gene product had activity to produce not only GM1 but GD1b (5), the resulting transfectant cells expressed increased levels of GM1 and fucosyl-GM1, and reduced levels of GT1b. Consequently, we could analyze the effects of GM1 derived from introduced cDNA on the response to NGF.

In the response to NGF, GM1$^+$ cells showed much reduced reaction in both the neurite extension and the activation of TrkA/ERK1/2 signaling pathway. The vector control cells showed fairly good neurite formation and prompt phosphorylation of TrkA upon NGF treatment. ERK1/2 were also activated quickly with a peak at 5 min after NGF treatment. In